



**KTH Chemical Engineering
and Technology**

Ring-opening catalysts for cetane improvement of diesel fuels

Ulf Nylén

Doctoral Thesis 2005

KTH – The Royal Institute of Technology
Department of Chemical Engineering and Technology
Chemical Technology
SE-100 44 Stockholm, Sweden



Ulf Nylén

Born 1975 in Stockholm, Sweden

M. Sc. (Chem. Eng.) 2001

The Royal Institute of Technology (KTH), Stockholm

TkL (Chem. Eng.) 2004

The Royal Institute of Technology (KTH), Stockholm

TRITA-KET R222

ISSN 1104-3466

ISRN KTH/KET/R--222--SE

ISBN 91-7178-221-4

Abstract

The global oil refining industry with its present product distribution essentially shifted towards fuels such as gasoline and diesel will most likely hold the fort for considerable time. However, conditions are changing and refinery survival will very much depend on long-term planning, process and product flexibility and being at the frontiers of refining technology, a technology where catalysts play leading roles. Today oil refiners are faced with the challenge of producing fuels that meet increasingly tight environmental specifications, in particular with respect to maximum sulphur content. At the same time, the average quality of crude oil is becoming poorer with higher amounts of aromatics, heteroatoms (sulphur and nitrogen) and heavy metals. In order to stay competitive, it is of decisive importance for refiners to upgrade dense petroleum fractions of low quality to highly value-added products. A practicable route, for example, is upgrading the catalytic cracking by-product Light Cycle Oil (LCO) into a high-quality diesel-blending component in a two-step catalytic process. In the first step the LCO is hydrotreated over a Pt-Pd-based acidic catalyst bringing about heteroatom and aromatic reduction and isomerization of C₆ to C₅ naphthenic structures. In the second step these naphthenic structures are selectively opened over an Ir-based catalyst to improve the cetane value.

The present thesis is mainly devoted to the second catalytic step of LCO upgrading and was partly conducted within the framework of the European Union project RESCATS.

From the patent literature it is evident that iridium-based catalysts could be good candidates for ring-opening purposes. A literature survey covering ring opening of naphthenic structures made in the beginning of the project (in 2001), showed the need for extending investigations to heavier hydrocarbons, more representative of the diesel fraction than model compounds such as alkylated mono C₅ and C₆ naphthenic rings frequently employed in previous academic studies.

Ring-opening catalysts, mainly Pt-Ir based, were synthesised at KTH by two different techniques: the microemulsion and the incipient wetness techniques. Paper I is a review of the microemulsion technique and its applications in heterogeneous catalysis. Characterization of catalysts was performed employing a multitude of techniques including quantitative TPR, TEM-EDX, XPS, CO FT-IR, NH₃-DRIFTS and XRF etc. Catalytic screening at 325 °C and atmospheric pressure with hydrogen and pure indan as model substance was conducted to investigate ring-opening activity in terms of conversion and selectivity to desired cetane-boosting products. This development process

is the topic of Papers **II-IV**. The possible industrial implementation of the best catalyst candidate is demonstrated in Paper **V**.

When designing a catalytic system aimed at refining petroleum, it is crucial to monitor the evolution of the sulphur distribution throughout the different stages of the process so that catalyst properties and reaction parameters may be optimised. The final section of this thesis and Paper **VI** are devoted to high-resolution sulphur-distribution analysis by means of a sulphur chemiluminescence detector (SCD) following gas chromatographic separation.

Keywords: ring opening (selective), naphthenic structure, indan, light cycle oil (LCO), cetane, Pt-Ir catalyst, microemulsion, XPS, TPR, TEM, DRIFTS, sulphur analysis, GC-SCD.

Sammanfattning

Den globala industrin för oljeraffinering med dess nuvarande produktinriktning mot främst drivmedel som bensin och diesel kommer säkerligen att ha en fortsatt stark ställning men förutsättningarna är på väg att förändras. Vilka raffinaderier som överlever kommer bero på graden av framförhållning, flexibilitet i produktutbud och processteknologi samt tillämpning av nya landvinningar inom raffineringstekniken, en teknik där katalysatorer spelar en avgörande roll. Idag står raffinaderinäringen inför utmaningen att tillverka drivmedel som uppfyller allt strängare miljökrav, i synnerhet när det gäller den maximalt tillåtna svavelhalten. Samtidigt blir den genomsnittliga råoljekvaliteten allt sämre med högre halter av aromatiska kolväten, kväve- och svavelföreningar samt tungmetaller. För att vara konkurrenskraftig är det absolut nödvändigt att kunna omvandla tyngre petroleumfraktioner av låg kvalitet till lönsamma produkter. Ett exempel är att genom en katalytisk process i två steg omvandla biprodukten från katalytisk krackning, Light Cycle Oil (LCO), till en dieselbränslekomponent av hög kvalitet. I första steget hydreras LCO över en Pt-Pd-baserad sur katalysator vilket medför en sänkning av heteroatom- och aromathalter samt isomerisering av C₆ till C₅ nafteniska strukturer. I det andra steget klyvs dessa nafteniska kolväten selektivt över en Ir-baserad katalysator för att förbättra slutprodukten cetanvärde.

Detta forskningsarbete fokuserar huvudsakligen på det andra katalytiska steget vid omvandling av LCO och utfördes delvis inom ramarna för det europeiska projektet RESCATS.

Av patentskrifter framgår att iridiumbaserade katalysatorer skulle kunna vara synnerligen användbara vid ringöppning. En litteraturoversikt avseende ringöppning av naftener visade i projektets inledningsskede år 2001 på behovet av att utöka undersökningarna till att inkludera tyngre kolväten, eftersom dessa är mer representativa för de molekyler som ingår i dieselbränslet än de alkylerade C₅ och C₆ nafteniska modellsubstanser som tidigare ofta använts i akademiska studier.

Katalysatorer för ringöppning, mestadels baserade på Pt-Ir, har tillverkats vid KTH med två olika metoder: mikroemulsions- respektive impregneringstekniken. Artikel I är en översikt över mikroemulsionstekniken och dess användningsområden i heterogen katalys. Karakterisering av katalysatorerna har gjorts med en rad tekniker, bland annat kvantitativ TPR, TEM-EDX, XPS, CO FT-IR, NH₃-DRIFTS och XRF etc. Katalytiska tester vid

325 °C och atmosfärstryck med vätgas och ren indan som modellsubstans utfördes för att studera ringöppningsförmåga vad gäller omsättning och selektivitet för önskvärda produkter med högre cetanvärden. Detta utvecklingsarbete är temat för artikel **II-IV**. Förutsättningarna att använda den bästa katalysatorkandidaten i industriella sammanhang visas i artikel **V**.

Vid utvecklandet av katalysatorer för oljeraffinering är det mycket viktigt att kunna följa hur fördelningen av svavelföreningar ser ut i olika skeden av processen så att katalysatoregenskaper och processparametrar kan optimeras. Den sista delen av avhandlingen samt artikel nummer **VI** ägnas åt högupplösande svavelfördelningsanalys med hjälp av en svavelkemiluminiscensdetektor (SCD) efter separation med gaskromatografi.

Nyckelord: ringöppning (selektiv), naftenisk struktur, indan, light cycle oil (LCO), cetan, Pt-Ir katalysator, mikroemulsion, XPS, TPR, TEM, DRIFTS, svavelanalys, GC-SCD.

List of papers

This doctoral thesis is based on the following publications, referred to by their capital Roman numerals. The papers are appended at the end of the thesis.

- I. *Preparation of catalysts from microemulsions and their applications in heterogeneous catalysis*
S. Eriksson, **U. Nylén**, S. Rojas, M. Boutonnet, Appl. Catal. A-Gen. 265 (2004) 207.
- II. *Low and high-pressure ring opening of indan over 2 wt.% Pt, Ir and bi-metallic Pt₂₅Ir₇₅/boehmite catalysts prepared from microemulsion systems*
U. Nylén, J. Frontela Delgado, S. Järås, M. Boutonnet, Appl. Catal. A-Gen. 262 (2004) 189.
- III. *Catalytic ring opening of naphthenic structures Part I. From laboratory catalyst screening via pilot unit testing to industrial application for upgrading LCO into a high-quality diesel-blending component*
U. Nylén, L. Sassu, S. Melis, S. Järås, M. Boutonnet, accepted for publication in Appl. Catal. A-Gen.
- IV. *Catalytic ring opening of naphthenic structures, Part II - in-depth characterization of catalysts aimed at upgrading LCO into a high-quality diesel-blending component*
U. Nylén, B. Pawelec, M. Boutonnet, J.L.G. Fierro, accepted for publication in Appl. Catal. A-Gen.
- V. *New effective ceria-based bimetallic precious metals ring-opening catalysts for diesel quality improvement, with special emphasis on cetane enhancement*
U. Nylén, registered in the office of the Spanish notary D. Carlos Solis Villa in Madrid on 2005-02-23 with the document reference no. 425 (English and Spanish versions)
Registered under “Pli soleau” at the office of the French National Institute for the Intellectual and Industrial Protection (INPI) in Compiègne on 2005-09-28 with the document reference no. 239913.
- VI. Characterization of alkylated aromatic sulphur compounds in light cycle oil from hydrotreated vacuum gas oil using GC-SCD
U. Nylén, J. Frontela Delgado, S. Järås, M. Boutonnet, Fuel Process. Technol. 86 (2004) 223.

Contributions to the publications

- I. The review is a joint effort between all the authors. However, in section 3. *Catalytic applications*, the authors put forward information related to his/her specific field of research. Consequently, I wrote sub section 3.1. *Hydrogenation, hydrogenolysis and isomerization catalysts*.
- II. I am the principal author of this paper. The high-pressure experiment with indan and the LECO analysis of the spent catalyst from the atmospheric pressure reaction were conducted at the CEPSA R&D Department in Madrid, Spain, by Dr Juana Frontela Delgado and her colleagues. Regarding catalyst characterization, I actively took part when Dr Gérard Bergeret, Dr Pierre Delichere and Dr Mimoun Aouine at the CNRS catalyst research institute in Lyon, France, performed the XRD, XPS and TEM-EDX analyses, respectively.
- III. I am the main author of this paper, however, significantly assisted by Lorenzo Sassu at the Process Department of Saras Ricerche e Tecnologie SpA who performed, evaluated data and wrote the text sections related to the high-pressure experiments. The characterization of spent catalysts from the atmospheric pressure reaction by TPO-TG-MS was performed at the CEPSA R&D Department. I directed and supervised the analyses, however, Dr José Maria Mazón Arechederra performed them physically.
- IV. I am the principal author of this paper. The XPS analyses were performed chiefly by Professor J.L.G. Fierro at the Catalysis and Petrochemistry Institute (ICP) in Madrid, Spain. He also conducted the FT-IR of adsorbed CO experiments. However, I did all the data evaluation. The XRF analyses were carried out by Francisca Salort Salom, previously at the CEPSA R&D analytical department.
- V. I am the author of this communication. I directed and performed the high-pressure experiments with the HDT-LCO at the CEPSA R&D Department. The physical and chemical characterization of the oil samples in terms of density, SIM-DIS, aromatics distribution, sulphur and nitrogen content were conducted by CEPSA's analytical department.
- VI. After starting up the non-functional GC-SCD equipment and revamping it to top-of-the-line conditions, I performed all the analyses and am the principal author of the article.

Conference and seminar contributions

- i. *The influence of the Pt particle size on the selective ring opening of indan*
U. Nylén, M. Boutonnet, S.Järås, Poster presentation / book of abstracts, 10th Nordic symposium on catalysis, Helsingør, Denmark, June 2-4, 2002.
- ii. *Selective ring opening of naphthenic rings for cetane number improvement*
U. Nylén, M. Boutonnet, S.Järås, Poster presentation / book of abstracts, 4th Tokyo conference on advanced catalytic science and technology, Tokyo, Japan, July 14-19, 2002.
- iii. *Selective ring opening of naphthenic molecules for cetane boosting*
U. Nylén, M. Boutonnet, S.Järås, Oral presentation, 2nd EFCATS school on catalysis, Tihany, Hungary, September 25-29, 2002.
- iv. *Selective ring opening of naphthenic rings for cetane number improvement*
U. Nylén, S.Järås, M. Boutonnet, Poster presentation / book of abstracts, 6th European congress on catalysis (EUROPACAT VI), Innsbruck, Austria, August 31 - September 4, 2003.
- v. *Characterization of aromatic sulphur compounds in light cycle oil (LCO) using GC-SCD*
U. Nylén, J. Frontela Delgado, S. Järås, M. Boutonnet, Accepted for oral presentation / book of abstracts, 13th Saudi-Japanese Symposium on Catalysts in Petroleum Refining & Petrochemicals, Dhahran, Saudi Arabia, December 14-15, 2003.
- vi. *Ring opening of naphthenic structures for diesel quality improvement*
U. Nylén, J. Frontela Delgado, S. Järås, M. Boutonnet, Oral presentation / book of abstracts, 19th North American Catalysis Society Meeting, Philadelphia, USA, May 22-27, 2005.

Table of contents

1 INTRODUCTION	1
1.1 Setting the scene	1
1.2 The petroleum industry – survey of present activities and future challenges	2
1.3 The diesel engine: principle of operation and fuel characteristics	5
1.4 The European RESCATS project: academia and industry working together on LCO upgrading	8
1.5 Scope of the present thesis	9
2 MODEL COMPOUNDS FOR INVESTIGATING RING-OPENING ACTIVITY	11
2.1 Methylcyclopentane	12
2.2 C ₁₀ & C ₁₁ bi-cyclic hydrocarbons	13
2.3 Indan	13
2.4 Model compounds employed in the RESCATS project	14
3 SYNTHESIS AND CHARACTERIZATION OF RING-OPENING CATALYSTS	17
3.1 The microemulsion technique	19
3.2 The incipient wetness technique	20
3.3 Catalysts prepared in connection with the present PhD studies	21
3.4 Characterization of Pt-Ir-based catalysts	22
3.4.1 Characterization of microemulsion catalysts	23
3.4.2 Characterization of incipient wetness catalysts	28
3.4.3 Miscellaneous characterization techniques employed	36
4 CATALYTIC BEHAVIOUR	39
4.1 Ring opening of indan at atmospheric pressure	39
4.1.1 Catalyst pre-treatment	39
4.1.2 Experimental apparatus and screening conditions	40
4.1.3 Catalytic results	40
4.2 Evaluation of the best catalyst candidate with the real feed HDT-LCO	46

4.2.1 <i>Experimental apparatus, catalyst pre-treatment and experimental conditions</i>	46
4.2.2 <i>Catalytic results</i>	48
5 SULPHUR IN PETROLEUM STREAMS	53
5.1 The need for sulphur characterization when refining petroleum.....	53
5.2 Analytical determination of sulphur compounds.....	54
5.3 Analysis conditions.....	57
5.4 Results.....	57
6 CONCLUSIONS	61
6.1 Summary of the present thesis	61
6.2 Looking ahead.....	63
7 ACKNOWLEDGMENTS.....	65
NOMENCLATURE.....	67
REFERENCES	69
APPENDICES: PAPERS I-VI	

1 Introduction

1.1 Setting the scene

The tremendous technical and social development taken place since the middle of the 19th century, is closely linked to the discovery, extraction and refining of oil. The sovereign control over fossil fuel reservoirs has been and still is the reason for numerous wars and uprisings all over the world. In the 1970s there were several serious oil crises caused by conflicts in the Middle East (e.g. the Arab/Israeli Yom Kippur war 1973, the Iranian revolution 1979 and the Iran/Iraq war starting 1980) and as a result, the price of crude oil increased drastically. For many countries this was an eye-opener that raised legitimate questions regarding our industrialized societies' vital dependence on oil for heating, power generation and transportation. As a result, the use of nuclear technology was intensified and nuclear power plants were set up at a hurried pace. Despite a well-developed technology with rigorous safety margins, accidents occurred at Harrisburg (US) in 1979 and Chernobyl (former USSR) 1986 and made the public aware of the severe, long-term consequences of wide-spread radioactive material from a reactor meltdown. With the exception of hydropower, the large-scale expansion of alternative technologies such as wind [1,2], solar [3], marine (e.g. tidal [4], wave [5], current [6]) and geothermal energy [7] and the development of cleaner and safer energy carriers such as biomass [8] and hydrogen [1,9] is underway but for the moment, their contributions are far too small. The fact is that our present high-standard way of living is to a large extent still dependent on an immense and regular supply of oil that inevitably brings about hazardous emissions when transformed.

In 1956, based on scientific estimates of US oil reserves and future oil production rates, the American geophysicist Dr M. King Hubbert predicted that the US oil production would culminate in the early 1970s. Almost everyone, inside and outside the oil industry, was sceptical of Dr Hubbert's ideas and thought that he was yet another crying wolf. In fact, the actual peak year turned out to be 1970 [10]. Around 1995, Hubbert's methodology was used again by several analysts, but now with the focus to predicting the

peak year for world oil production. On average, the results indicated that a maximum would occur between 2004 and 2008 [11]. According to estimations published this year by BP [12], proven reserves of the fossil fuels oil, natural gas and coal worldwide will, if taking into account current production rates, last for approximately 41, 67 and 164 years, respectively.

The societal transition from fossil fuels to renewables has only just begun and liquid fossil hydrocarbon mixtures such as gasoline and diesel will remain the key transportation fuels for many years to come [13-15]. Consequently, research in the field of oil refining technology is still very important. In many refining operations catalysts play a key role and even minor improvements in activity and selectivity may be of considerable value taking into account the vast number of barrels that are processed every day worldwide.

1.2 The petroleum industry – survey of present activities and future challenges

Although energy conservation and the development of alternative energy systems and infrastructures for future energy carriers are crucial issues, the oil refining industry will continue to play an important role in the foreseeable future. However, its activities will be controlled and governed by increasingly strict environmental legislation and, to meet future requirements, many refineries will be forced to substantial revamping or investments in new technology. In addition, to be competitive the refinery of tomorrow must be able to process crude oils of variable quality and have the flexibility to easily shift the product composition when demanded [16]. It is no overstatement to say that the refining industry is facing big challenges.

As a consequence of the accelerating production rates during the 20th century the average quality of the oil extracted from easily accessible oil fields on and off shore has become poorer, i.e. higher in density and with increased amounts of heteroatoms such as sulphur and nitrogen. With the “low-hanging fruit already plucked”, oil companies have to search for new locations to drill. Around 75 % of the estimated oil and gas reserves lie offshore, frequently in remote and hostile regions and the industry has been forced to move into increasingly deep water to tap the deposits [17]. Promising areas on shore include Southern Russia, the Middle East and North and West Africa [18].

Before entering the field of oil refining technology, a few words must be said about natural gas and its growing role as a generator of heat and power beside, of course, its importance as raw material for the petrochemical industry. In contrast to coal and oil,

natural gas is considered to be a clean fuel. The composition of natural gas depends on the specific reservoir but, in general, it mainly contains low molecular-weight hydrocarbons of which methane is the major constituent. Sulphur levels are often extremely low which is a positive characteristic in view of future chemical application. In the steam-reforming process natural gas is converted into hydrogen and carbon monoxide, both desirable products for further production of chemicals, for example in the synthesis of synthetic high-quality diesel fuel via the Fischer-Tropsch process [19]. Exploitation and extraction of natural gas are gradually increasing and, in contrast to oil, the reserves are not concentrated to the Middle East region [12]. In addition, considerable amounts of methane are trapped in water cages of different structures, known as clathrate hydrates [20]. However, natural gas and methane can neither answer to our soaring demand for energy in compliance with sustainability.

As of January 1, 2004 there were 717 oil refineries worldwide with a total capacity of 82.055 million barrels per calendar day (b/cd), i.e. slightly more than 13 million m³/day. The continental refinery distribution was Asia 200, North America 159, Western Europe 104, Eastern Europe 95, South America 69, Middle East 46 and Africa 44 [21]. The top ten list of oil refiners is presented in Table 1.1.

A modern refinery is a highly complex industrial plant with the purpose of efficiently converting crude oil with high yields into profitable products such as liquid petroleum gas (LPG), gasoline, jet and diesel fuels, wax, lubricants and bitumen. Low molecular-weight

Table 1.1 Ranking of the world's largest oil refiners [21]

Rank	Company	Crude refining capacity	
		(b/cd) ^a *10 ⁶	(m ³ /day) *10 ⁵
1	ExxonMobil Corp.	5.30	8.42
2	Royal Dutch/Shell Group	4.82	7.66
3	BP PLC	3.29	5.22
4	Petroleos de Venezuela SA	2.67	4.25
5	Sinopec	2.67	4.24
6	ConocoPhillips	2.60	4.13
7	Total SA	2.60	4.13
8	ChevronTexaco Corp.	2.18	3.47
9	Saudi Aramco	2.15	3.41
10	Petroleo Brasileiro SA	1.93	3.07

^a barrels per calendar day

products (methane, ethylene, propylene, iso-butene etc.) are further used as building blocks in the petrochemical industry. However, gasoline, diesel and non-transportation fuels account for 75-80 % of the total refinery products [22]. A general outline of a modern refinery is presented in Fig. 1.1.

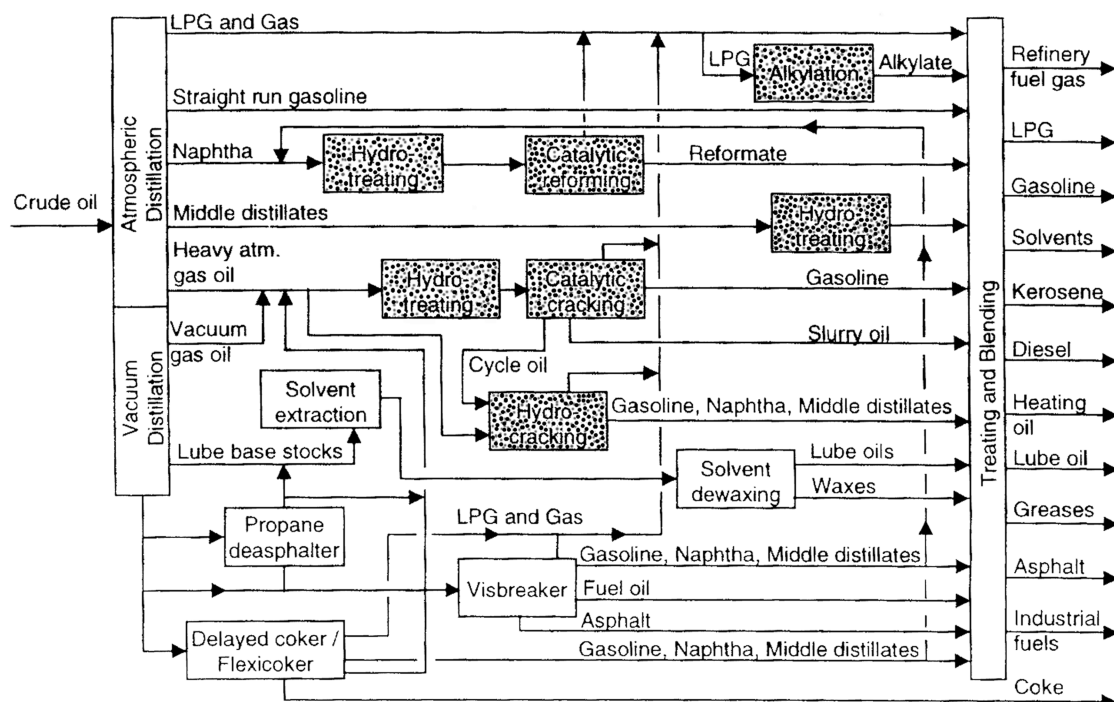


Figure 1.1 Flow scheme of a complex modern oil refinery [23]. Boxes with dots represent processes where catalysts are employed.

The crude oil is fractionated in atmospheric and vacuum distillation units and the streams (cuts) are subsequently subjected to different chemical refining techniques of varying severity. In many of these unit operations catalysis plays a crucial role, for example in hydrotreating (HDT), reforming, alkylation, hydrocracking, fluid catalytic cracking (FCC) and dewaxing, see Fig. 1.1. Oil refining catalysts and related catalytic processes are big business with major actors such as Akzo Nobel Catalysts BV, Axens, BASF, Criterion Catalyst Company LP, Engelhard Corporation, Haldor Topsoe AS, Universal Oil Products (UOP) and Zeolyst International. In the wake of increasing sales of refining catalysts together with more stringent environmental laws on hazardous waste, the market for reclamation of metals, rejuvenation and reuse of spent discarded catalysts is also growing [24].

Today the refining industry has to process heavier and heavier feedstocks and refiners have to look for new alternatives to improve economic margins with the increasing share of middle distillates. In Europe, the diesel engine car has during the last decade gained more and more ground compared to its gasoline-fuelled counterpart due to its superior fuel economics (on average 30 % less fuel required and 25 % less CO₂ produced) and the implementation of new effective exhaust gas filters that drastically reduce the emission of particulate matter (PM). Moreover, the diesel fuel has traditionally a lower basic cost, a higher volumetric heat content and, in many countries, a significantly lower tax. According to the European automobile manufacturers association (ACEA) [25], in 2004 almost every second newly-registered passenger car (48.9 %) in the 15 member states of EU was equipped with a diesel engine, compared to 23.1 % in 1994. Consequently, the refining industry needs additional capacity to meet the steadily increasing demand for high quality diesel fuel. One interesting option is to upgrade Light Cycle Oil (LCO) into a high quality diesel-blending component. LCO is the residue stream from the FCC unit and is normally disposed of as low-value heating oil. It is characterized by a high content of aromatics (> 70 wt.%) and a relatively high amount of heavy aromatic sulphur and nitrogen compounds (~3 and 0.08 wt.%, respectively) [26]. LCO upgrading may be achieved by a two-step catalytic process involving hydrotreatment and isomerization followed by selective ring opening (SRO) of naphthenic structures resulting in a product with a reduced content of sulphur, nitrogen and aromatics and with an increased cetane number [27,28]. The cetane number is an important diesel fuel parameter that affects the self-ignition behaviour.

1.3 The diesel engine: principle of operation and fuel characteristics

In the 1890s when Rudolf Diesel (1858-1913) developed the diesel engine, his objective was to achieve greater thermal efficiency by utilization of a higher expansion ratio, by increasing the compression ratio, which, at the same time, produced a temperature high enough to cause the fuel to ignite spontaneously when injected into the hot compressed air. Nowadays, an arbitrary diesel engine may operate at compression ratios of about 20:1 and by employing the Common rail technique the diesel fuel is introduced at approximately 1800 bar as an aerosol into the cylinders. Such high-pressure fuel pumps are relatively expensive and an average diesel vehicle is generally more costly than one running on gasoline. The cost is also due to the higher complexity that requires sophisticated electronic management systems for fuel injection, ignition timing and emissions control. The high temperatures achieved in a diesel engine not only improve the thermal efficiency but also favour the formation of NO_x since ordinary air is

employed in the combustion process. Together with soot formation, this has been the major drawback of diesel engines. Pollutants abatement is an important issue chiefly driven by progressively tougher legislation [29].

Diesel fuel is defined as a hydrocarbon mixture containing straight-chain alkanes (paraffins), saturated cyclic structures (naphthenes) and aromatics, boiling in the range 210 – 340 °C [30]. In a refinery, several streams are blended into the diesel pool, e.g. straight-run gas oil and gas oil from the hydrocracking and the FCC processes.

As briefly mentioned previously, the performance of a diesel engine is significantly affected by the fuel quality in terms of auto-ignition behaviour. As opposed to gasoline in a spark-ignition “Otto” engine, the diesel fuel must ignite spontaneously and with minimal delay when introduced to the hot, highly compressed air in the combustion chamber. This delay is expressed by the cetane value: the higher the cetane the shorter the lag between injection and ignition. The cetane number (CN) of a fuel is determined in a standardised test engine procedure (ASTM D613) employing reference mixtures of *n*-hexadecane (CN=100) and heptamethylnonane (CN=15). In practice, the compression ratio in the engine is varied to give the same ignition delay period for the fuel and the two reference blends of higher and lower quality than the test fuel. Once the compression ratio required by the actual fuel has been bracketed, the cetane number may be calculated by interpolation. Owing to the expense of the cetane number test, correlating empirical formulas based on certain physical properties of the diesel fuel have been developed. The cetane index (CI) according to ASTM D4737 is calculated on the basis of the sample density and various temperature values from its simulated distillation (SIM-DIS) curve and the agreement with the CN is reported to be very good [31]. The most marked effects associated with poorer ignition quality fuels (lower cetane values) are related to higher combustion noise, i.e. “diesel knock”, due to uncontrolled burning rates when combustion finally starts implying high rates of pressure rise and high peak pressures [32]. As a consequence, low cetane values have been reported to yield higher emissions of CO, unburned hydrocarbons (HC), NO_x and PM [33].

Table 1.2 lists the cetane number of some important hydrocarbon classes and petroleum fractions. α -Methylnaphthalene used to represent the bottom of the cetane scale but has been replaced by heptamethylnonane due to its higher stability [34]. It is clearly seen that the cetane number is very poor for FCC cycle oil (0-25). To be used as a diesel-blending component, the cetane of the FCC stream must be boosted significantly. According to the current European Union diesel specifications, a cetane number of at least 51 is required [35]. The development of European Union diesel fuel specifications is detailed in Table 1.3.

Other important diesel fuel parameters include cold-flow properties such as viscosity and cloud point (related to amount of wax), flash point, total content of aromatics, volatility etc. Concerning production of diesel fuels (and gasoline) the focus today is mainly set on lowering the sulphur levels and stricter and stricter specifications are to be expected [27,36,37]. When combusted, organic sulphur species are transformed into sulphur oxides (SO_x) that contribute to acidification. In addition, sulphur-free fuel is necessary for catalytic NO_x converters to operate satisfactorily [38]. However, sulphur does not only have negative effects. It acts as a lubricant, which is positive for engine performance by minimizing engine wear. As fuel sulphur levels are gradually lowered, lubricant additives must be added.

Table 1.2 Cetane numbers of various hydrocarbon classes and of main refinery gas oil streams (typical ranges) [28]

Hydrocarbon class	Cetane number
<i>n</i> -Hexadecane (cetane)	100 ^a
<i>n</i> -Alkanes	100-110
<i>iso</i> -Alkanes	30-70
Alkenes	40-60
Cyclo-alkanes	40-70
Alkylbenzenes	20-60
Naphthalenes	0-20
α -Methyl naphthalene	0 ^a
Straight-run gas oil	40-50
FCC cycle oil	0-25
Thermal gas oil	30-50
Hydrocracking gas oil	55-60

^a by definition

Table 1.3 Past, present and future diesel fuel specifications in the European Union [14,35]

Year	1996	2000	2005	2009
Sulphur, max (ppm(wt))	500	350	50/10 ^a	10
Cetane number, min	49	51	51	51
Polyaromatics, max (wt.%)	-	11	11	11
Density 15 °C (kg/m ³), max	860	845	845	845
95 % distillation point (°C), max	370	360	360	360

^a “...by no later than 1 January 2005 diesel fuel with a maximum sulphur content of 10 mg/kg must be marketed and be available on an appropriately balanced geographical basis within the territory of a Member state.” [35]

- No limit

Sweden has since long been well positioned regarding production of environmentally friendly, high-quality diesel fuel. In January 1991, as one of the first countries in the world, environmental classification of diesel fuels for use in urban areas was introduced [32]. There are three oil refineries in Sweden that produce transportation fuels, all of them located on the West coast. In contrast to other European refineries they have an excess capacity for diesel production due to limited national demand and much of the diesel fuel is exported. The largest refinery, Scanraff in Lysekil, has recently invested some 370 million € in a new mild hydrocracker (an ISO cracker from Chevron) together with a hydrogen generation plant in order to increase the capacity for “sulphur-free” high-quality diesel fuel (<10 ppm(wt) S) at the expense of heavy heating oil [39]. Shortly after that announcement, the Finnish oil consortium Fortum presented an even larger investment with the same purpose in their refinery in Sköldvik [40]. Both plants are expected to be up running in 2006. These examples clearly illustrate that production of clean diesel fuels from low-value oil fractions is very attractive from an industrial point of view and hence, pioneering research in this area is in demand.

1.4 The European RESCATS project: academia and industry working together on LCO upgrading

In 2001 a three-year European Union research project entitled “Poison-resistant catalysts for clean diesel production from LCO” was launched. The division of Chemical Technology at KTH was one out of seven participants including two universities, two research institutes, two refineries and a catalyst manufacturer. The members covered all aspects required in the development process from catalyst synthesis and primary screening, via pilot unit evaluation to large-scale catalyst formulation and industrial

implementation. The scientific approach was to employ a two-step catalytic process involving hydrotreatment and isomerization over a Pt-Pd-based acidic catalyst followed by selective (catalytic) ring opening (SRO) of naphthenic structures resulting in a product with a reduced content of sulphur, nitrogen and aromatics and with an increased cetane value.

The KTH role in the project included chiefly synthesis, characterization and catalytic screening at atmospheric pressure of ring-opening catalysts aimed at the second cetane-boosting step. The starting point was to systematically investigate bimetallic systems based on platinum (Pt) and other precious metals, e.g. iridium (Ir), rhodium (Rh) and ruthenium (Ru). However, since it is well known that noble metal-based catalysts are negatively affected by the presence of sulphur in the feed, another important task assigned to the KTH group was to analyse the sulphur distribution in relevant petroleum streams by means of a highly sensitive sulphur chemiluminescence detector (SCD) coupled to a gas chromatograph (GC).

1.5 Scope of the present thesis

The material presented in this thesis sets out from the ideas of the RESCATS project. The starting point is the literature survey covering ring opening of model naphthenic structures and it clearly shows that in the beginning of 2001 there was a gap with respect to heavy naphthenic and aromatic-naphthenic hydrocarbons, indan in particular. The desired reaction, selective ring opening, requires the use of noble metal-based catalysts of which iridium (Ir) proves to be a metal of particular interest. The catalysts were prepared employing two different techniques: initially focusing on the microemulsion technique but as time went on shifting over to the more simple, and for this application superior, traditional incipient wetness method. The catalysis takes place on the surface of the catalyst and in order to understand the chemistry involved, knowledge of surface properties is essential. During six months (September 2004 – February 2005) the author stayed in Madrid, Spain and worked on a daily basis at the former RESCATS partner CEPESA's R&D department in Torrejón de Ardoz and the Institute of Catalysis and Petrochemistry (ICP) in Cantoblanco. Consequently, an extensive body of material was gathered that has been essential to the successful achievement of correlations between catalytic ring-opening performance in terms of activity, i.e. conversion of indan, and specific surface characteristics such as metal dispersion and amount of carbonaceous deposits. The catalytic performance of noble metals is, in general, inhibited by the

presence of sulphur species. In the final chapter, characterization of the sulphur distribution in relevant petroleum streams is presented and discussed, framed against the backdrop of catalyst development and the urgency of thio-resistance.

2 Model compounds for investigating ring-opening activity

The majority of refinery streams are complex mixtures of many different hydrocarbons and fuels classification is usually based on boiling point ranges. As previously mentioned, diesel fuel is defined as a fraction boiling between 210 and 340 °C [30]. However, to gain insight on a fundamental level with respect to target reactions, the systems have to be simplified and hence model substances are commonly employed in laboratory investigations.

Before going into details, the definition of the target ring-opening reaction must be clarified since it is reported in the literature by various terms. The aim is to bring about selective ring opening (SRO) of naphthenic rings, cleaving only one endocyclic C-C bond so that reduction of molecular weight is avoided, resulting in products having higher cetane values than the initial saturated ring species. Identical to SRO but with a broader meaning, the term hydrogenolysis refers to a type of reaction in which the rupture of an arbitrary bond A-B is accompanied by addition of hydrogen to both A and B [41].

Ring opening and hydrogenolysis as well as hydrogenation are all exothermic reactions. According to thermodynamics, an exothermic reaction is not favoured by high temperatures, but the reaction kinetics, which is determined by the specific rate constant given by the Arrhenius equation will conversely be positively affected. In other words, there will be an optimal reaction temperature. Pushing the thermodynamic equilibrium in favour of the forward reaction to obtain larger equilibrium constants may be achieved, as predicted by Le Chatelier, if the pressure is increased. These fundamental principles are illustrated in Fig. 2.1 for hydrogenation of aromatics.

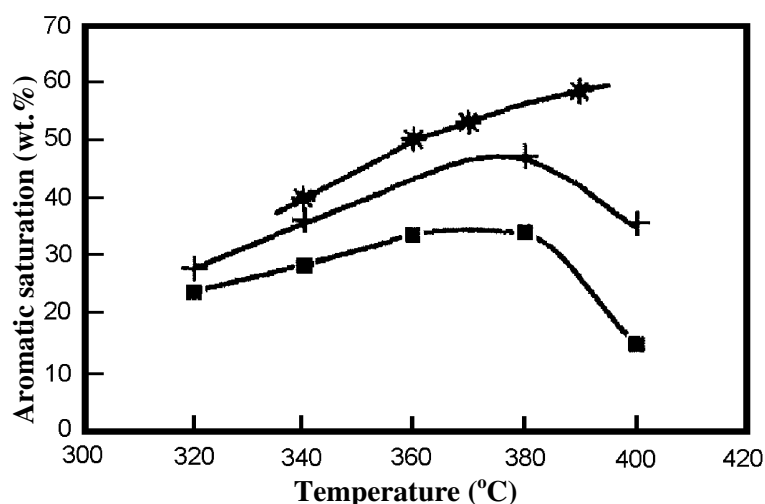


Figure 2.1 Aromatic saturation as a function of reactor temperature and pressure on a Middle East heavy gas oil: ■, 4.5 MPa; +, 6.5 MPa; *, 12.5 MPa [42].

The following sub-sections (2.1-2.3) describe the most common ring-opening model substances found in the literature.

2.1 Methylcyclopentane

Selective ring opening has mostly been investigated using mono C₅ naphthenic rings, non or alkyl branched, as model substances. Ring opening of methylcyclopentane (MCP) for example is a well-documented reaction. Catalysts based on noble metals from Group VIII such as Pt, Ir, Rh and Pd deposited onto various supports successfully convert MCP into a mixture of C₆ alkanes. Depending on the active metal employed, this reaction is known to be either structure sensitive or insensitive [43]. In the case of Pt the reaction is structure sensitive, i.e. the particle size affects the product selectivity; on highly dispersed Pt ($d_p < 2$ nm) the reaction follows the non-selective mechanism where the products 2-methylpentane (2-MP), 3-methylpentane (3-MP) and *n*-hexane (*n*-Hex) are formed in statistical distribution 2:1:2 whereas on Pt of “lower dispersion” ($d_p > 2$ nm) the reaction follows the selective mechanism with the 2-MP to 3-MP ratio equal to 2 [44]. Over Ir and Rh the MCP reaction follows the selective mechanism [45,46-47], whereas for Pd the non-selective mechanism prevails [48]. Apart from its selective catalytic behaviour in MCP ring opening, iridium is also well known for its high hydrogenolysis activity. Multiple splitting (cracking) readily occurs and increases with temperature [49]. When investigating upgrading of heavy petroleum streams to diesel fuel, MCP is not an adequate model hydrocarbon since it has a boiling point of only 72 °C, which is far below the diesel range.

2.2 C₁₀ & C₁₁ bi-cyclic hydrocarbons

Several papers have been presented in recent years dealing with the development of catalysts (both precious and non-precious metal based) for upgrading of heavy petroleum fractions. The model substances employed have almost exclusively been heavy bi-C₆-cyclic hydrocarbons such as decalin [50-56], tetralin [54-68], naphthalene [68-74] and methyl-substituted naphthalenes [75-77]. Based on reaction stoichiometry considerations, the majority of these studies were carried out at elevated pressure and at a temperature between 200 and 400 °C. The product distribution becomes more and more complex with increasing number of carbon atoms in the reactant molecule and products have to be divided into subclasses. In this context it is important to emphasize that mass spectrometry following separation by on-line gas chromatography (GC) is essential if reaction mechanisms are to be revealed. For example, in-depth studies of decalin ring opening presented by Kubička et al. [51,52] have demonstrated that skeletal isomerization over Brønsted acid sites into alkyl-substituted bicyclononanes and bicyclooctanes is a fundamental, consecutive step preceding the ring-opening reaction. However, they concluded that ring opening may take place both on Brønsted acid sites and on metal crystallites, e.g. Pt. In a pioneering work by McVicker et al. [53], it was clearly shown that among the metals Pt, Ir, Ru, Rh and Ni, Ir was the most active and selective metal with respect to cleaving unsubstituted C-C bonds in naphthenic five and six-membered rings. In agreement with the previously cited work of Kubička, it was also shown that direct ring opening of a C₆ naphthenic structure is much slower than that of a C₅ naphthenic ring owing to substantially lower ring strain of the former. Consequently, the ease of converting two-ring naphthenes containing combinations of C₅ and C₆ structures over Ir-based catalysts is directly related to the relative number of C₅ rings in the molecule. Furthermore, it was demonstrated that the addition of alkyl substituents has a negative effect, in general, on activity and selectivity due to steric hindrance. In essence, ring opening may preferentially be investigated employing a molecule containing at least one C₅ naphthenic framework.

2.3 Indan

The hydrotreating catalyst operating in the first RESCATS step (see end of section 1.2) was suggested to include a noble metal alloy (Pt-Pd) deposited on an acidic support. Besides enhancing the sulphur tolerance, the acidity of the support would bring about ring contraction of intermediate C₆ naphthenic structures into C₅ alkyl substituted naphthenic structures. It is well established that C₅ rings are more readily opened up than their C₆

counterparts due to substantially higher ring strain [53]. The molecular structure of indan is a C₅ naphthenic ring adjacent to a benzene ring and it was thus considered to be a suitable model substance despite the fact that the boiling point is somewhat too low (176 °C) and thus below the diesel range. In marked contrast to the C₁₀ and C₁₁ model hydrocarbons discussed in section 2.2, the literature on catalytic ring opening of indan is very limited and the investigations were all performed a long time ago in the 1960-70s [78-81]. These articles, however, were initially very valuable for estimating reaction parameter settings as well as for building GC methods and identifying reaction products.

2.4 Model compounds employed in the RESCATS project

The work presented in this thesis has been carried out within the frame of the RESCATS project where the process outline was a two-step configuration with essentially different prerequisites and objectives. For the second ring-opening step, model substances proposed in the project description were indan and “indanes”. In spite of this, one

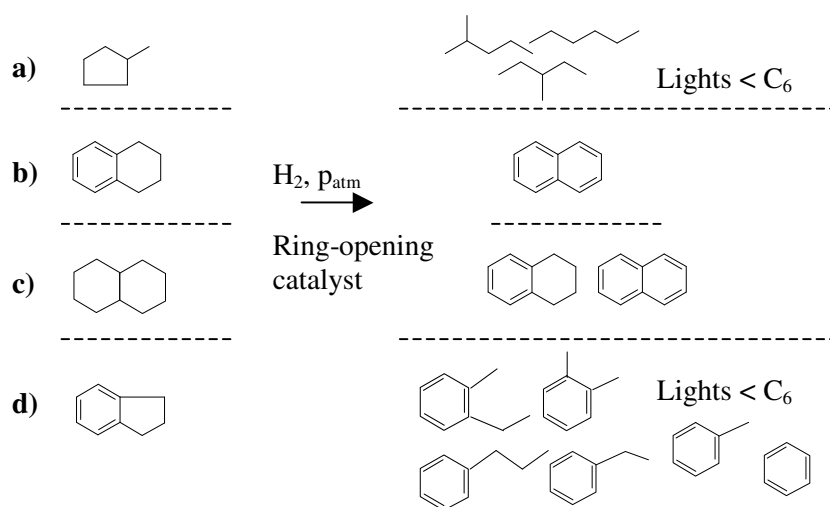


Figure 2.2 Reaction schemes for the tested cyclic model substances at atmospheric pressure conditions:

- a) MCP ring opening with products (in order of appearance) 2-methylpentane, 3-methylpentane, *n*-hexane and lights
- b) tetralin is dehydrogenated into naphthalene
- c) decalin is also dehydrogenated (mostly into naphthalene)
- d) ring opening of indan resulting in 2-ethyltoluene, *n*-propylbenzene, and further dealkylation into *o*-xylene, ethylbenzene, toluene, benzene and extensive fragmentation (lights).

standard feed mixture consisting of 40 wt.% tetralin in *n*-hexadecane (*n*-cetane) spiked with 50 ppm (wt) S from dibenzothiophene was eventually chosen as common model feed.

During the initial start-up period several cyclic model hydrocarbons were tested in the newly constructed continuous fixed bed atmospheric pressure reactor. The reactions are presented in Fig. 2.2, demonstrating the major reaction products obtained as determined by GC-FID (Flame Ionization Detector).

Ring opening of MCP and indan proceeded in agreement with results reported in the literature. Several attempts were made to run with both tetralin and decalin but they resulted almost exclusively in undesired dehydrogenation into naphthalene. Consequently, and in accordance with the original scientific ideas, the decision was made to proceed with pure indan in the gas phase. The use of a model substance facilitates the investigation of catalytic behaviour and it often serves as a sufficient means in the early selection process. The most interesting aspect, however, is the catalyst candidate's performance when exposed to the real HDT-LCO feed. Key parameters studied included sulphur distribution and content, density, average boiling point, aromatic distribution and content, cetane value (CN/CI) and nitrogen content. For adequate comparisons to be made it is essential that tests are performed similarly. The pilot units at the two partner refineries were checked at an early stage of the project and good consistency between results was obtained, all things equal. However, during evaluation of catalyst candidates, different HDT-LCO feeds were employed.

3 Synthesis and characterization of ring-opening catalysts

Owing to its intrinsically high hydrogenolysis/hydrogenation activity [49,82], iridium is an obvious active-component candidate when considering catalyst formulas to be employed for upgrading heavy petroleum fractions. Its supremacy is clearly illustrated by several patents issued recently [83-87]. Another attractive property of iridium is that when introduced into a hydrocarbon refining catalyst, formation of carbonaceous deposits is tempered and deactivation is markedly slowed down [88-90]. In general, a catalyst manufacturing company sells not only the catalyst, rather a whole licence. The terms vary but the license may include deliverance, pre-treatment and on-stream protocols, performance support and regeneration procedures and eventually discarding. In other words, the basic cost of the catalyst itself is of minor importance, but definitively not negligible. The price trend of Ir and some other noble metals often encountered in catalysis is presented in Fig. 3.1.

As suggested by the RESCATS project description, Pt-Ir should be the composition to

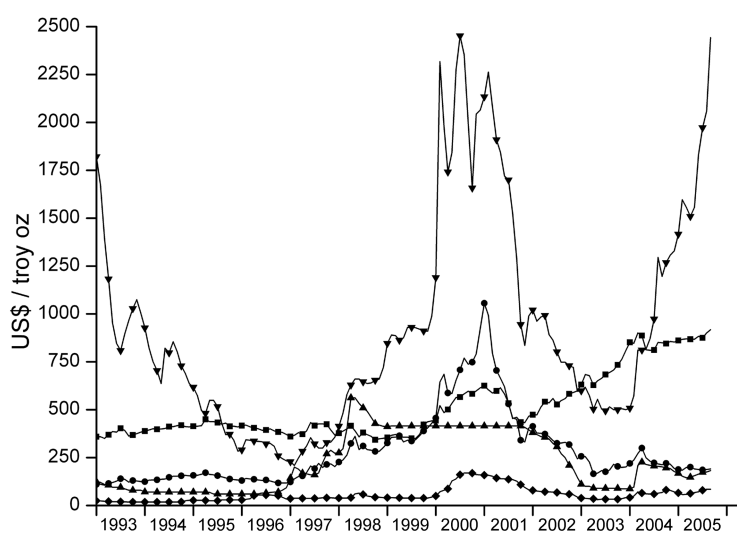


Figure 3.1 The price trend of Ir (▲), Pt (■), Rh (▼), Pd (●) and Ru (◆) [91]. (1 troy oz = 31.1 g)

focus on. It is well established that sulphur in the feed stream will have a negative impact on the performance of a noble mono-metallic catalyst but the discovery of sulphur-tolerant Pt-Pd alloy catalysts for aromatics hydrogenation [42,92], indicated that alloying may perhaps enhance sulphur tolerance in other refining areas as well. Moreover, the inclusion of a certain amount of Pt would temper the high hydrogenolysis activity of Ir, creating a more selective ring opener that would mitigate fragmentation. Also the choice of support material was defined to be an important parameter. A large number of different carriers were employed throughout the project; from normal standard supports such as alumina and titania provided by the French company CTI (Céramiques Techniques et Industrielles) in Salindres, to newly developed supports such as tungstated zirconia [93] and various pillared layered clay materials [94]. Important characteristics of a support material include specific surface area (BET) and pore size distribution, morphology (extent of amorphousness/crystallinity), thermal stability, acid/base character and strength (particularly that of Lewis/Brønsted acidity) and for industrial applications also mechanical properties such as crush strength and loss on attrition, etc. The way the catalyst is prepared, the pre-treatment and the activation procedures will also affect its final catalytic properties. There are several techniques for synthesizing catalysts and in the following sections the two methods employed during the RESCATS project are presented.

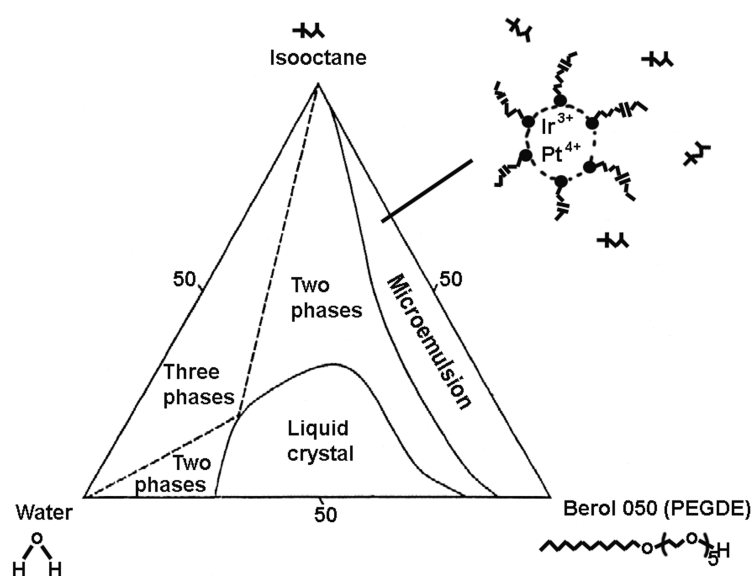


Figure 3.2 A schematic ternary phase diagram of the microemulsion system employed

Table 3.1 Principal microemulsion systems employed during the RESCATS project

	Water phase ^a (wt. %)	Oil phase, isooctane (wt. %)	Surfactant, PEGDE (wt. %)
Formula 1	5	75	20
Formula 2	15	23	62

^a Including 2 wt.% noble metal(s)

3.1 The microemulsion technique

A microemulsion is defined as a system consisting of water, a hydrocarbon solvent and a surfactant. It is an optically isotropic and thermodynamically stable solution that hence looks homogeneous but is in fact heterogeneous at the molecular level. Depending on the component concentration, the microemulsion may consist of small, uniformly sized droplets that are shielded either by the surfactant molecules' hydrophilic or hydrophobic tails. A schematic ternary phase diagram is presented in Fig. 3.2 and illustrates that the three constituents must be carefully balanced in order to achieve a microemulsion, as several rheologies are possible. Moreover, it is important to bear in mind that the actual features of such ternary phase diagrams depend on the oil and surfactant species employed, the temperature and pressure.

In the early 1980s it was discovered that metallic particles could be prepared conveniently from water-in-oil (w/o) microemulsions. Upon incorporation of soluble metal precursor salts into the tiny well-defined water micelles and subsequent reduction with a powerful reducing agent such as hydrazine or hydrogen, metal particles with a narrow size distribution may be obtained [95]. However, the particle formation has been shown to proceed in two steps: first nucleation inside the droplets and secondly particle growth by agglomerate collisions due to the system's dynamic character. The size of the water droplets may be altered by varying the water-to-surfactant ratio, ω . An increase of ω at constant concentration of surfactant will increase the average diameter of the droplets. However, the rate of particle growth is predominantly governed by the concentration of surfactant: an increase (at a constant water-to-oil ratio) will yield smaller and more numerous droplets in the first place and secondly affect the coalescence process by steric hindrance. The ability to tailor small nano particles of narrow size distribution, hence with a very high metal accessibility, is an important tool, in particular if the catalyst is to

be utilized in structure sensitive reactions. Moreover, the method allows for the preparation of alloy particles at room temperature [96].

The microemulsion technique and its applications in heterogeneous catalysis are delved into in Paper I (a review on the topic).

Two microemulsion systems were employed in the RESCATS project and these are presented in Table 3.1.

The starting point was formula 1 which is an in-house developed standard recipe at the division utilized to prepare nano-sized particles of Pt. The water phase contained chiefly water-soluble chloridic salts such as $\text{IrCl}_3 \cdot 3\text{H}_2\text{O}$ and $\text{H}_2\text{PtCl}_6 \cdot 6\text{H}_2\text{O}$ that had previously been dissolved separately in deionised water to contain 2 wt.% of the noble metal. The non-ionic surfactant Berol 050 (pentaethylene glycol mono *n*-dodecyl ether, PEGDE) and the hydrocarbon solvent isooctane (2,2,4 trimethylpentane) were vigorously shaken before adding the water phase. The majority of microemulsion catalysts prepared were synthesized according to formula 2 with a higher amount of surfactant. Reduction of the precursor ions was carried out either using hydrazine or hydrogen; the support was added either before or after reduction. THF (tetrahydrofuran) was in most cases used to destabilize the microemulsion system in order to transfer the particles onto the support. The catalyst was washed with ethanol three times with intermediate centrifugation and eventually dried. It is obvious that a vast number of synthesis parameters may be altered. For example, the microemulsion constituents and their relative composition, synthesis temperature and pressure, addition order of ingredients, type and addition procedure of reducing agent, destabilisation agent, drying procedure and thermal post treatment and activation protocols.

In spite of its attractive features, the microemulsion method has not yet been adopted industrially mainly due to difficulties related to depositing the nanoparticles onto the support avoiding particle agglomeration, the large amounts of waste chemicals that have to be separated before being recycled and limited catalyst batch sizes.

3.2 The incipient wetness technique

Due to its simplicity this is one of the most common techniques for catalyst preparation. A metal precursor-containing impregnation solution (often water-based) is added to a well-dried support in an amount just sufficient to fill the pores and wet the outside of the

support particles. The impregnation solution is allowed to dry completely whereupon metallic precursors deposit on the support as the solvent evaporates. The final metal loading of the catalyst as well as the particle size is controlled by the concentration of metal in the impregnation solution. All catalysts prepared in the present work were based on 2 wt.% aqueous solutions. The incipient wetness technique should not be confused with the wet impregnation technique where the support is contacted with a large volume of impregnation solution long enough to attain equilibrium. The metal loading is determined by measuring the difference in metal concentration in the impregnating solution before and after contacting. According to Xue et al. [97] who prepared Pt-Ir/Al₂O₃ with these two methods and investigated whether alloy-type clusters were formed or not by studying temperature-programmed reduction (TPR) traces, the incipient wetness technique was superior and created close intimacy between the two metals.

3.3 Catalysts prepared in connection with the present PhD studies

During the course of the RESCATS project 45 different ring-opening catalysts were synthesized in the division laboratory. Out of these 45 catalysts, 31 were prepared employing the microemulsion technique and 14 were made via the incipient wetness method. After the completion of the RESCATS project, another 10 incipient wetness catalysts were prepared. Following the RESCATS project description for the first year, a large number of bimetallic Pt₅₀-M₅₀ (M=Ir, Ru, Rh, Pd, Os, Co, Au, In, La and Ni) catalysts were prepared via the microemulsion technique. The nominal metal loading was 2 wt.%, that is, a value commonly found in the literature. The principal support material employed initially was boehmite, a precursor to alumina.

Based on catalytic results, Pt-Ir combinations appeared to be most appropriate and were subsequently deposited on common support materials including alumina (γ -Al₂O₃), zirconia (ZrO₂), ceria (CeO₂, containing 20 wt.% alumina as binder), silica (SiO₂), silica-alumina (SiO₂-Al₂O₃), magnesia (MgO) and titania (TiO₂). Although common supports, most of them had never been used for ring-opening purposes. Additionally, many newly developed supports were tested such as Al-NNB (aluminium pillared layered montmorillonite-type clay), MCM-36 (mesoporous aluminosilicate), FSM-10,16 (folded silica material with supposedly very high surface area ~1000 m²/g), H-SA (acid treated saponite), S-ZrO₂ and W-ZrO₂ (super acidic supports). Among all these support materials, the ceria carrier appeared most promising. At this time, it was also well established that for this particular application, there were no advantages employing catalysts prepared via the microemulsion technique (formula 1 or 2). Among the final

catalysts, a series of 2 wt.% Pt_xIr_y/CeO₂ catalysts (x=0, 5, 15, 25, 50, 100; y=1-x) was prepared via incipient wetness, and these were to contribute to the most significant results of this thesis.

Based on the ring-opening performance with indan at atmospheric pressure, taking into account chiefly the level of conversion (since selectivity did not vary significantly), the four most promising catalyst candidates were prepared on a larger scale (~ 30 g) and sent to one of the two refineries involved in the RESCATS project for high-pressure evaluation with model substances and the real feed HDT-LCO.

3.4 Characterization of Pt-Ir-based catalysts

Catalysis is a phenomenon occurring on surfaces and for a deeper understanding of how the catalysed reaction de facto proceeds and is enabled, surface characterization but also complementary bulk characterization are valuable tools for the catalyst researcher. Bimetallic Pt-Ir catalysts are not new to the catalysis community, but they have not yet been used for naphthenic ring-opening purposes. In the early 1970s, Exxon Research and Engineering Company introduced Pt-Ir/Al₂O₃ catalysts in their naphtha reforming units for octane enhancement [98]. Since then, several papers have been put forward presenting details on both catalytic reforming performance and catalyst structure using characterization techniques such as XRD (X-Ray Diffraction) [99,100], Mössbauer spectroscopy [101], H₂ and CO chemisorption [99,100,102,103], Laser Raman spectroscopy [104] and EXAFS (Extended X-ray Absorption Fine Structure) [105,106]. Another technique employed frequently is TPR [97,107-114]. However, results differ markedly and peak positions, peak features and their chemical interpretation have been subjects of lively discussion. In general, supported metal clusters pose a challenge in terms of characterization since they are small, usually nonuniform, and present in only low loadings (usually a few tenth of a wt.% to about 3-4 wt.%) in solids that are frequently amorphous. The best approach is hence to combine results from several characterization techniques.

As pointed out by McVicker et al. [53], selective ring opening of naphthenic rings is a metals-driven chemistry. A certain surface area is of course needed for spreading out the active metal components. However, a simple calculation based on molar weights, specific metallic surface areas of platinum and iridium and Avogadro's number shows that in order to distribute the present 2 wt.% metal loading evenly over the support as isolated accessible surface atoms, the support needs only a specific surface area of approximately

4.9 and 4.8 m²/g for platinum and iridium, respectively. Due to the moderate temperatures employed in the catalytic reactors (the upper limit being 450 °C) there will neither be problems related to thermal sintering. Consequently no emphasis will be put in the following sections on the characteristics of the support materials in terms of specific surface area and pore size distribution as all but one support material (rutile titania) have BET specific surface areas well exceeding the required values.

The following sections will present the most significant characterization results. Information regarding various instruments, parameter settings, sample-preparation procedures and data evaluation techniques are fully detailed in the experimental sections of Papers II-IV.

3.4.1 Characterization of microemulsion catalysts

One of the first characterization techniques employed was Scanning Electron Microscopy with accompanying Energy Dispersive X-ray Spectroscopy (SEM-EDX). The microscopy displays the surface topography and an estimation of particle size, shape and size distribution may be achieved but the resolution is restricted to approximately 5 nm [115]. The EDX is a powerful tool that enables spot detection of elemental composition by varying the section area of the impinging electron beam. Fig. 3.3 a) presents a picture of the 2 wt.% Pt₂₅Ir₇₅/boehmite catalyst “as prepared”. The white spots reveal the existence

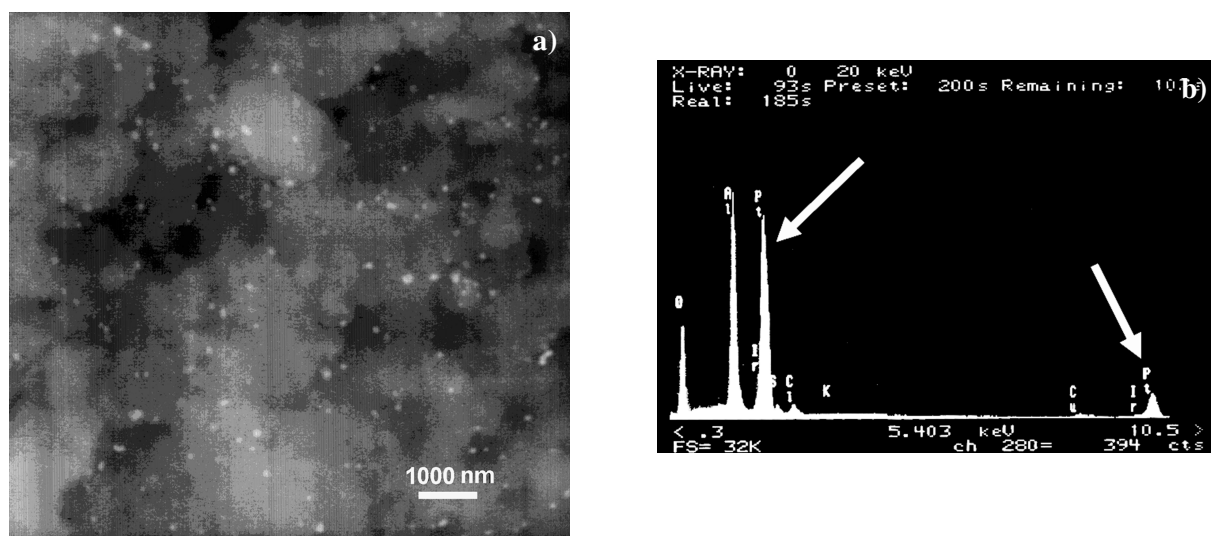


Figure 3.3 SEM-EDX results for the 2 wt.% Pt₂₅Ir₇₅/boehmite ME catalyst “as prepared”:

- a) SEM survey picture
- b) EDX analysis of one of the white spots seen in a)

of unexpectedly large metal agglomerates in the range 50-100 nm, although well distributed over the surface. EDX analysis in the centre on one of those spots shows an overwhelming presence of platinum, see Fig. 3.3 b).

Similar to SEM, Transmission Electron Microscopy (TEM) gives an electron-mediated picture of the sample topography and particularly metal particles, their size, shape and distribution are conveniently studied. In general, a resolution of a few Ångström is obtainable, however, today's top-of-the-line instruments are capable of presenting pictures with a resolution below 0.7 Å [116]. Nevertheless, when information is acquired from such small regions of sample, caution must be taken when drawing conclusions concerning the state of the whole material. A repeated analysis of different sample areas and subsequent statistical evaluation give the most reliable results.

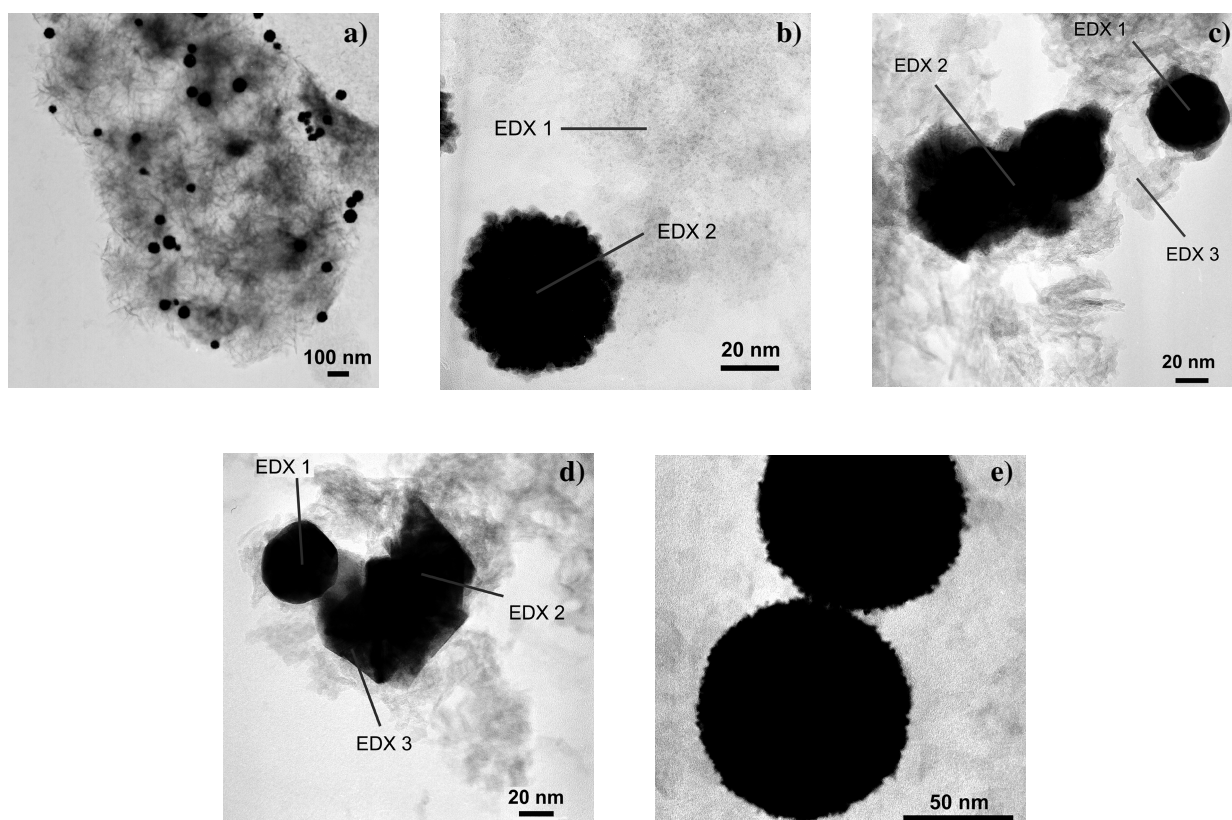


Figure 3.4 TEM pictures of various 2 wt.% Pt_xM_y /boehmite microemulsion catalysts:
a,b) $Pt_{25}Ir_{75}$ “as prepared”
c,d) $Pt_{25}Ir_{75}$ additionally reduced in flowing H_2 for 1 h at 450 °C
e) $Pt_{50}Rh_{50}$ “as prepared”

Table 3.2 Elemental composition of the 2 wt.% Pt₂₅Ir₇₅/boehmite ME catalyst as determined by EDX

	Atomic concentration (%)			
	O	Al	Ir	Pt
Figure 3.4 b)				
EDX 1	53.4	44.6	1.8	0.2
EDX 2	27.9	12.5	0.9	58.7
Figure 3.4 c)				
EDX 1	17.3	3.4	0.0	79.4
EDX 2	59.9	2.3	13.5	24.3
EDX 3	76.5	9.7	13.3	0.6
Figure 3.4 d)				
EDX 1	34.4	18.1	0.0	49.7
EDX 2	56.8	13.8	2.6	27.1
EDX 3	68.7	12.8	16.9	0.6

In Fig. 3.4 a-e), five representative TEM-EDX pictures taken of 2 wt.% Pt_xM_y/boehmite microemulsion catalysts are on display and together with the accompanying EDX results given in Table 3.2, the previous results from SEM are verified. Samples “as prepared” display large agglomerates of platinum metal in the range 20-100 nm (a,b,e)). Iridium is de facto present (Fig. 3.4 b), EDX-1) but the absence of visible particles suggests that the precursor IrCl₃ has not been properly reduced by hydrazine. In other words, the initial expectation that the reduction of Ir (and also Rh) would be mediated by the more easily reducible Pt came out unrealised.

After additional reduction of the sample in flowing H₂ at 450 °C precise EDX mapping revealed that the Pt₂₅Ir₇₅ catalyst in addition to the large agglomerates of platinum metal (Fig. 3.4 d, EDX-1) now also contained platinum agglomerates (EDX-2) lying on top of plates/sheets of iridium metal (EDX-3). This was an unexpected and interesting discovery indicating that the catalytic reaction might proceed differently along the Pt-Ir borderline.

The 2 wt.% Pt₂₅Ir₇₅/boehmite ME catalyst was furthermore checked with the surface-sensitive X-ray Photoelectron Spectroscopy (XPS) technique to obtain information regarding elemental surface composition and oxidation states by examining the magnitude of peak shifts. Fig. 3.5 shows the 4f levels of Ir and Pt to the left and right,

respectively. The tiled spectra demonstrate the catalyst in its fresh (“as prepared”), reduced (in situ XPS at 450 °C with flowing H₂) and spent (after the ring-opening reaction with indan at atmospheric pressure and 325 °C) states. The spectra are energy referenced to Al 2p at 74.5 eV and the deconvolution of the Ir 4f region into 10 % Lorentzian-Gaussian functions takes into account the interfering K $\alpha_{3,4}$ satellite lines due to the nonmonochromatic irradiation source employed. The major peak in the right hand side spectrum of Fig. 3.5 is Al 2p.

It is clearly seen in Fig. 3.5 that with respect to the Ir precursor, hydrazine is not a satisfactory reducing agent as the Binding Energy (BE) for the Ir 4f_{7/2} is equal to 62.7 eV which is exactly the value reported in the literature for IrCl₃ [117]. On the other hand, and in agreement with the observations from SEM-EDX and TEM-EDX, the Pt 4f_{7/2} line at 71.1 eV evidences the presence of metallic Pt [118]. Upon reduction at 450 °C, the Ir 4f_{7/2} peak shifts down to 61.1 eV indicative of metallic Ir (Ir⁰=60.9 eV [118]) whereas Pt stays unaffected. After the atmospheric pressure ring-opening reaction with indan, the spent sample was transferred to and stored in an air-containing scintillation jar. According to the literature [119], Ir is known to oxidize very easily and this was indeed observed, there

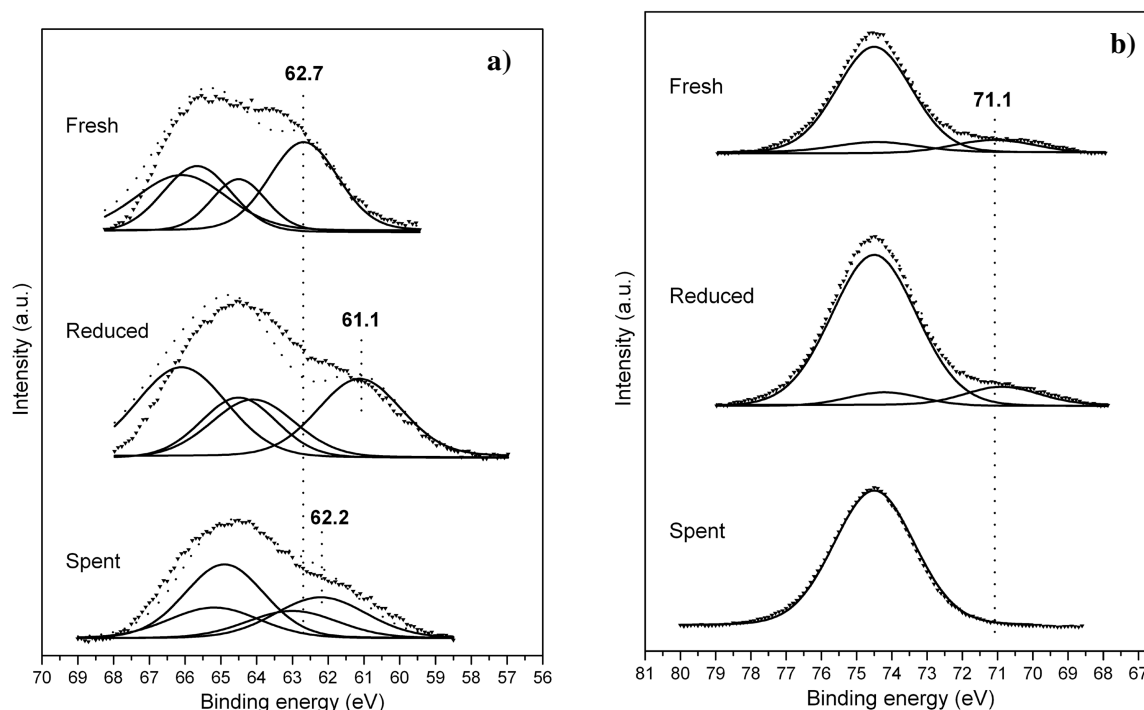


Figure 3.5 XPS spectra of the 2 wt.% Pt₂₅Ir₇₅/boehmite ME catalyst in its fresh, reduced (in situ XPS at 450 °C) and spent (after the p_{atm} reaction) states:

- a) Ir 4f
- b) Pt 4f

is also an upward shift to 62.2 eV for the Ir 4f_{7/2} indicating strongly the presence of IrO₂ [120]. Interestingly, after the hydrocarbon reaction the Pt 4f_{7/2} line disappears. Since metallic Pt is known to be extremely difficult to oxidize [121], the primary explanation would hence be coke coverage. However, considering the less intense 4d level, fitting of the Pt 4d_{5/2} and Pt 4d_{3/2} lines may readily be performed and the position of the former at 316.0 eV suggests the presence of PtO₁₋₂ (PtO=315.3 eV, PtO₂=317.0 eV [122]). Partial oxidation of Pt at room temperature may only be enabled by the presence of Ir and considering the TEM pictures in Fig. 3.4 d), the reaction may initially be triggered at and then further emanating from the Pt-Ir borderline.

Regarding the quantitative results, the Ir/Al and Pt/Al ratios in fresh, reduced and spent samples are 0.009, 0.006, 0.004 and 0.01, 0.008, 0.001, respectively. In contrast to the bulk composition measured by X-ray Fluorescence Spectroscopy (XRF) which was shown to be 1.9 wt.% Pt₂₅Ir₇₅, the surface Pt/Ir molar distribution is closer to 1 for all but the spent sample where there is four times more Ir. In chapter 4 it will be proved that a monometallic Pt catalyst is far more easily covered with coke than is its Ir counterpart. Consequently, this four-time drop indicates that the bimetallic homogeneousness is rather poor, which is fully in line with the observations from SEM-EDX and TEM-EDX.

Finally, it was also established that the sample contains both bulk and surface chlorine: according to the previous sequence denomination, the Cl/Al surface ratio was seen to diminish from 0.037 to 0.030 to 0.025. The corresponding bulk value obtained from XRF on the fresh sample was 0.020.

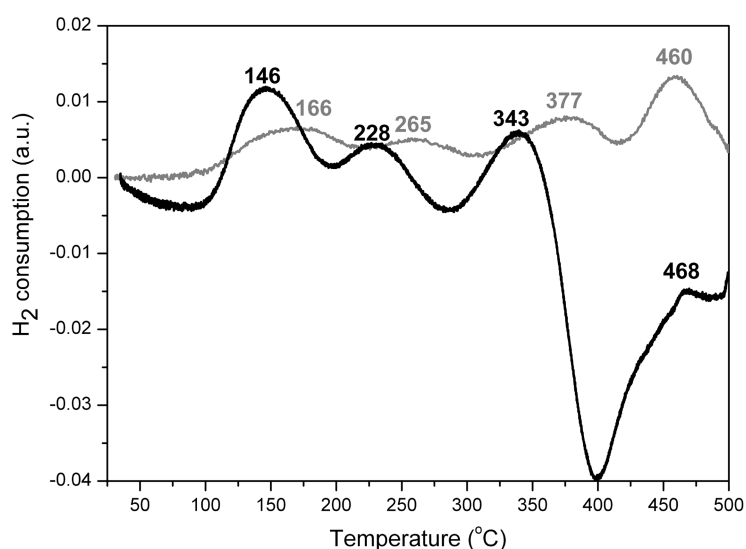


Figure 3.6 TPR traces obtained on the 2 wt.% Pt₂₅Ir₇₅/boehmite microemulsion catalyst “as prepared”.

Temperature Programmed Reduction (TPR) was conducted in order to study the reactions taking place during sample reduction, i.e. mimicking the in-situ reduction protocol prior to the catalytic reaction. In Fig. 3.6, traces of the 2 wt.% Pt₂₅Ir₇₅/boehmite ME catalyst “as prepared” are presented. For both runs, the analysis method was the same but the grey trace was obtained on approximately 50 mg pulverous sample whereas the black trace was obtained for approximately 200 mg of 0.12<d_p<0.25 mm particles employed in the atmospheric pressure catalytic reaction.

Based on the results from XPS, SEM-EDX and TEM-EDX, reduction of the Pt precursor has already been completed. In a separate run, it was checked that the boehmite support itself did not have any hydrogen uptake capacity that might interfere. In contrast to the TPR traces obtained for incipient wetness catalysts, which will be presented in the next section, the microemulsion catalysts display rather complex reduction behaviour. Although somewhat different, it is possible to distinguish four separate peaks in the TPR traces in Fig. 3.6. Quantitative determination of consumed hydrogen gas becomes speculative due to difficulties drawing an appropriate baseline. Nevertheless, the results from XPS confirm complete reduction of Ir at 450 °C.

Immediately after the TPR run, dynamic CO pulse chemisorption was performed at room temperature. It must be emphasized that the present method takes into account both chemically and physically adsorbed probing gas molecules and results may be somewhat overestimated but the method is sufficient for a relative comparison. Surprisingly, the Pt₂₅Ir₇₅/boehmite ME catalyst displays fairly good results. For the sake of clarity, values have been calculated both for the experimental XRF and the theoretical metal content values, the latter will be presented in brackets. The starting point for future calculations is the CO uptake value, which was 47.5 μmol/g catalyst. Consequently, the following results were obtained: accessible metallic surface area: 131 (127) m²/g metal; metal dispersion 54 (52) %; CO/M (M=Pt+Ir) molar ratio 0.47 (0.46); active mean particle size 2.06 (2.12) nm. Upon comparison with the TEM pictures in Fig. 3.4 a-d), the CO chemisorption results appear rather contradictory. It must be remembered though, that TEM is a strictly local method whereas CO chemisorption yields average information about the sample as a whole.

3.4.2 Characterization of incipient wetness catalysts

In the TEM picture a) in Fig. 3.7 of the Pt₂₅Ir₇₅/boehmite catalyst previously reduced at 450 °C, no particles could be detected. However, EDX analysis in this particular zone

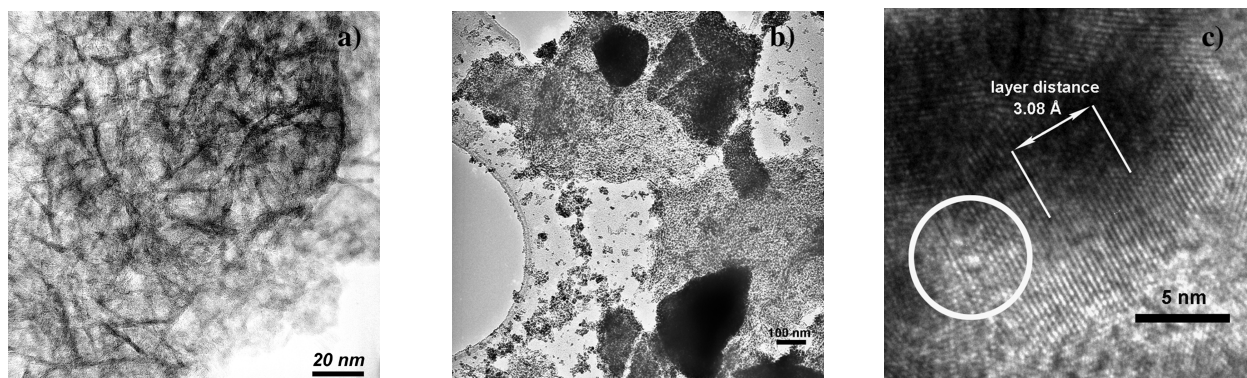


Figure 3.7 TEM pictures of 2 wt.% $\text{Pt}_x\text{Ir}_y/\text{support}$ catalysts prepared via the incipient wetness technique:

- a) $\text{Pt}_{25}\text{Ir}_{75}/\text{boehmite}$ reduced at 450 °C
- b) $\text{Pt}_5\text{Ir}_{95}/\text{CeO}_2$ reduced at 400 °C
- c) $\text{Pt}_5\text{Ir}_{95}/\text{CeO}_2$ reduced at 450 °C

showed that both Pt and Ir are present with an atomic Ir/Pt ratio of 0.31/0.11~3, a value corresponding with that obtained from XRF with respect to the bulk composition. Discerning possible noble metal particles in samples containing Ce is obstructed by cerium's relatively high molecular weight ($Z=58$) that also yields darker regions, clearly seen in Fig. 3.7 b) as large lumps. Noble metal particles could consequently not be detected in this particular study. However, the high-resolution picture c) obtained for the 2 wt.% $\text{Pt}_5\text{Ir}_{95}/\text{CeO}_2$ catalyst previously reduced at 450 °C shows some very interesting features. The ceria support is clearly seen as an ordered structure with a layer distance of 3.08 Å, which is very close to the 3.17 Å reported in the literature for CeO_2 (1 1 1) [123]. Yet, the most interesting detail is the marked particle within the drawn white circle that clearly breaks the ordered harmony, located on top of the ceria support. The particle has a diameter of 0.7 nm, which is in good agreement with the calculated average particle size based on dynamic CO pulse chemisorption measurements.

Concerning XPS spectra obtained from IW catalysts, similar shifts of the Ir $4f_{7/2}$ line as those observed for the microemulsion catalyst in Fig. 3.5 a) are observed between fresh, reduced and spent states, see Fig. 3.8 a). The peak intensities of the Ir $4f_{7/2}$ and its spin-orbit counterpart Ir $4f_{5/2}$ are now much larger than the satellite peaks, which is chiefly caused by the lower content of Al as the ceria support contains “only” 20 wt.% alumina as binder. Nevertheless, the Al 2p line causes severe shadowing of the Pt 4f level, which may only be adumbrated for reduced samples. Consequently, Pt had to be evaluated employing the less intense 4d level. In fact, information on surface Pt could only be

acquired for $\text{Pt}_{x \geq 25}\text{Ir}_{\leq 75}$ samples. In marked contrast to the boehmite-based ME catalyst, the ceria-based catalysts show a pronounced surface enrichment in Ir, as illustrated in Fig. 3.8 b) for the $\text{Pt}_{50}\text{Ir}_{50}$ sample. The Pt/Al surface ratio, however, remains almost equal to the corresponding bulk value throughout the various states. In general (as evidenced in Paper IV, Table 6), the position of the Pt $4d_{5/2}$ line is seen to shift from an, initially, relatively high BE most likely associated with the metal chloride, down to an average of 315.0 eV after reduction signifying, as expected, the presence of metallic Pt ($\text{Pt}^0 = 314.6$ eV [124]). This positive shift of 0.4 eV may be attributed to well dispersed metallic Pt [125], which is indeed corroborated by the results from CO chemisorption (Table 3.4). However, for Ir such a positive shift is only seen for the monometallic catalyst and the CO chemisorption results do not indicate a sudden deterioration in dispersion when introducing Pt. Interestingly, the Pt $4d_{5/2}$ line in spent bimetallics once again takes an intermediate position indicative of PtO_{1-2} species whose formation must be mediated by Ir and the existence of a close metals intimacy, i.e. an alloy-type phase, whereas Pt in the monometallic Pt catalyst remains unoxidized. In addition, for these bimetallics no drastic decrease is seen in the Pt/Al ratio between reduced and spent samples implying less carbonaceous deposits. Implicitly, this further indicates the existence of a more homogeneous bimetallic phase.

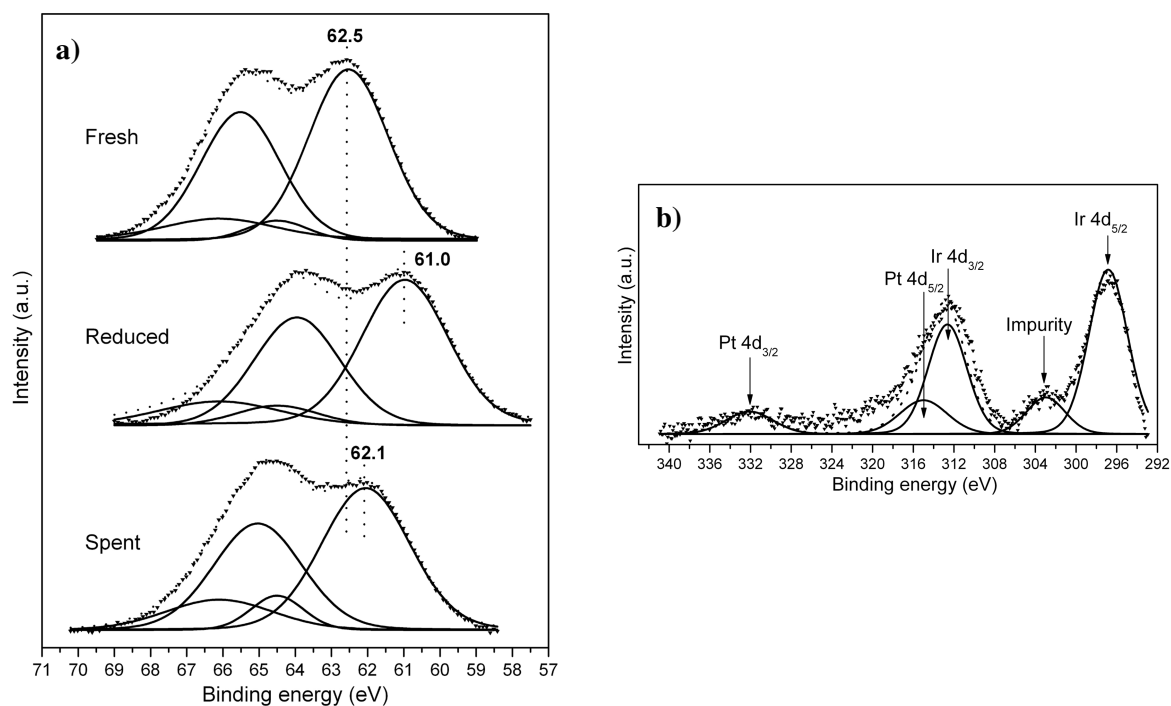


Figure 3.8 XPS spectra of 2 wt.% $\text{Pt}_x\text{Ir}_y/\text{CeO}_2$ catalysts:

- a) $\text{Pt}_{25}\text{Ir}_{75}$ fresh, reduced (in situ XPS at 400 °C) and spent (after the p_{atm} reaction), the Ir 4f level
- b) $\text{Pt}_{50}\text{Ir}_{50}$ reduced (in situ XPS at 400 °C), the Pt and Ir 4d level

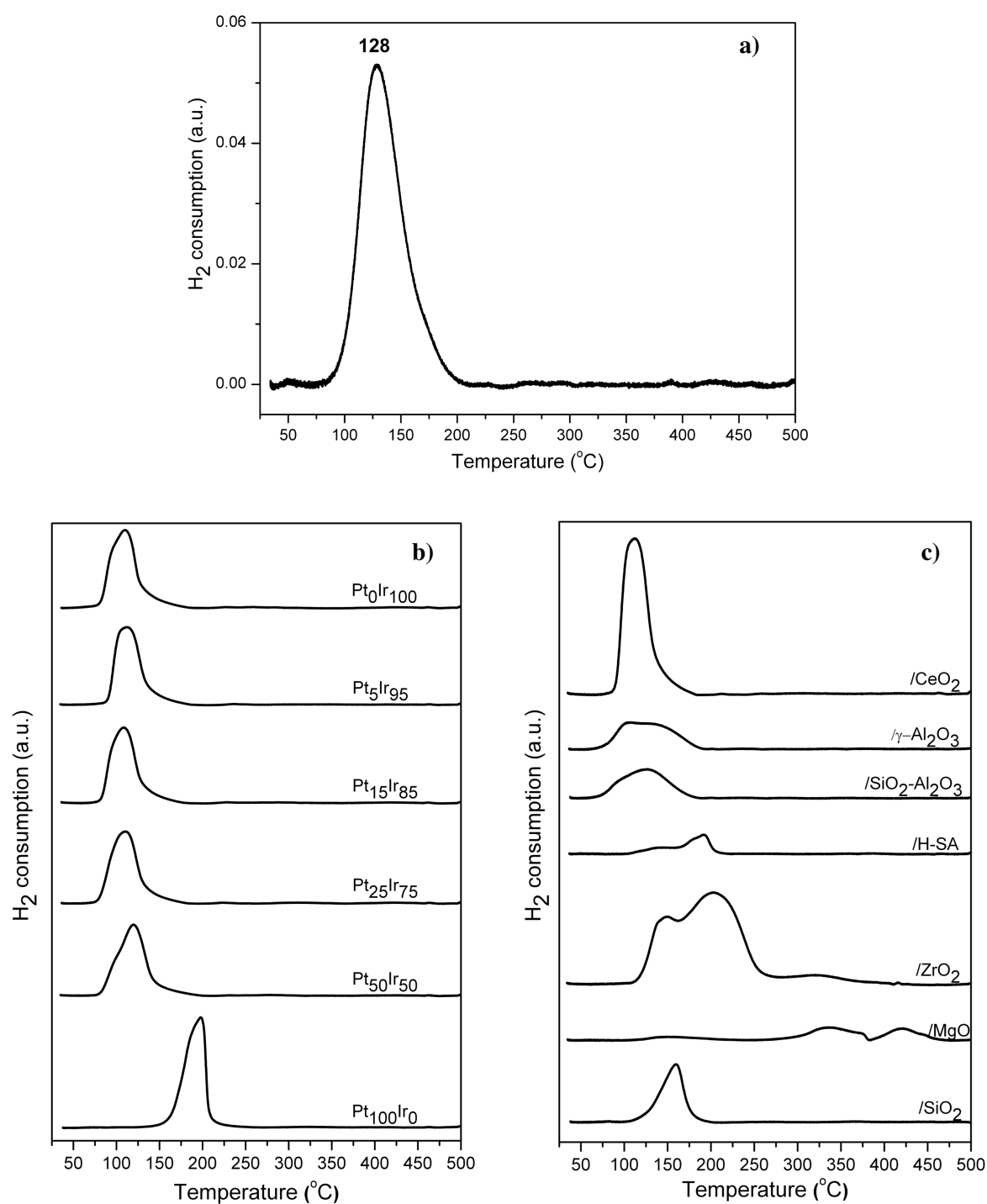


Figure 3.9 TPR traces for various 2 wt.% noble metal loaded catalysts prepared from the incipient wetness technique:
a) 2 wt.% $\text{Pt}_{25}\text{Ir}_{75}$ /boehmite
b) $\text{Pt}_x\text{Ir}_y/\text{CeO}_2$
c) $\text{Pt}_5\text{Ir}_{95}$ /support

In Fig. 3.9 a-c), the TPR traces for the most interesting IW catalysts are detailed. Peak characteristics together with results from the accompanying quantitative determination of the uptake of hydrogen, comparing actual values with theoretical and those based on XRF data required for complete reduction are given in Table 3.3. In marked contrast to the ME catalyst presented in Fig. 3.6, the TPR trace of its IW counterpart shown in Fig. 3.9 a) presents a completely different behaviour with a single peak at 128 °C. The area corresponds to a hydrogen uptake value of 181 $\mu\text{mol/g}$ catalyst which is slightly higher than the theoretical value but considerably lower than that based on XRF data regarding the content of noble metals. For ceria-based catalysts presented in Fig. 3.9 b) the peak position for the monometallic Pt catalyst is shifted +88 °C with respect to the monometallic Ir catalyst. The peak position values and the magnitude of the shift are in fair agreement with the findings of de Leitenburg et al. [126] who investigated similar systems. Importantly, the traces of the bimetallics are clearly not the sum of their individual Pt and Ir constituents and this observation is generally taken as a strong evidence of Pt-Ir alloy formation [97,107,109,111]. In agreement with the results from

Table 3.3 Trace characteristics and quantitative results from the TPR experiments

Catalyst	Peak position (°C)	H ₂ vol. uptake (cm ³ (n)/ g catalyst)	H ₂ molar uptake ($\mu\text{mol}/$ g catalyst)	H ₂ consumption required for complete reduction into M ⁰ ($\mu\text{mol/g}$ catalyst) ^a	
				Based on XRF data	Theoretical
2 wt.% Pt ₂₅ Ir ₇₅ /boehmite	128	4.06	181	218	168
2 wt.% Ir/CeO ₂	110	12.77	570	155	156
2 wt.% Pt ₅ Ir ₉₅ /CeO ₂	112	12.55	560	125	159
2 wt.% Pt ₁₅ Ir ₈₅ /CeO ₂	108	12.22	545	165	164
2 wt.% Pt ₂₅ Ir ₇₅ /CeO ₂	111	12.51	558	161	168
2 wt.% Pt ₅₀ Ir ₅₀ /CeO ₂	120	12.61	563	179	181
2 wt.% Pt/CeO ₂	198	13.16	587	179	205
2 wt.% Pt ₅ Ir ₉₅ / γ -Al ₂ O ₃	106, 135	3.28	146	162	159
2 wt.% Pt ₅ Ir ₉₅ /SiO ₂ -Al ₂ O ₃	98, 126	3.11	139	162	159
2 wt.% Pt ₅ Ir ₉₅ /H-SA	142, 181, 192	1.89	84	70	159
2 wt.% Pt ₅ Ir ₉₅ /ZrO ₂	149, 203, 322	18.28	815	172	159
2 wt.% Pt ₅ Ir ₉₅ /MgO	150, 338, 421	3.36	150	251	159
2 wt.% Pt ₅ Ir ₉₅ /SiO ₂	159	3.86	172	150	159

^a Assuming that the reduction of IrCl₃ and H₂PtCl₆ into their metallic states requires $n_{\text{H}_2}=n_{\text{Ir}}*1.5$ and $n_{\text{H}_2}=n_{\text{Pt}}*2$, respectively.

XPS where Ir was shown to have promoted the oxidation of Pt in spent, air-exposed catalysts, the TPR results evidence that Ir promotes the corresponding reduction reaction as well. The actual hydrogen consumption for the ceria-based catalysts are all approximately of the same magnitude and far exceed the amount required for complete metals reduction. This behaviour is also seen for the zirconia-based catalyst that has the highest hydrogen uptake value of all examined catalysts. The abundant hydrogen uptake observed is due to hydrogen spillover [127]. Upon reduction the metallic phase enables hydrogen dissociation and henceforth hydrogen atoms “spill over” and migrate out over the catalyst surface and cause partial surface reduction into substoichiometric phases of CeO_x [128] and ZrO_x [129]. These phases become progressively mobile with increasing temperature and result in various degrees of metals decoration. Concomitantly, Cl^- ions originating from the impregnation mother lye become progressively incorporated into the support lattice, substituting the oxygen atoms and highly stable oxychlorides (CeOCl) are formed [130]. However, the oxychloride phase is unstable in air and as evidenced by the quantitative XPS results detailed in Paper IV (Tables 6 & 7), the Cl^- ion substitution is a reversible reaction.

Table 3.4 Results from the dynamic CO pulse chemisorption experiments. Columns divided in two parts show values based on experimental XRF data to the left and those based on theoretical values to the right in brackets

Catalyst	CO uptake ($\mu\text{mol/g}$ catalyst)	$\text{SA}_{\text{metallic}}$ (m^2/g catalyst)	$\text{SA}_{\text{metallic}}$ (m^2/g metal)	CO/M (M=Pt+Ir) molar ratio	Dispersion (%)	Average particle size (nm)
2 wt.% $\text{Pt}_{25}\text{Ir}_{75}/\text{boehmite}$	45.6	2.4	94 (122)	0.34 (0.44)	39 (50)	2.9 (2.2)
2 wt.% $\text{Pt}_5\text{Ir}_{95}/\gamma\text{-Al}_2\text{O}_3$	74.5	4.1	199 (204)	0.70 (0.72)	83 (85)	1.3 (1.3)
2 wt.% $\text{Pt}_5\text{Ir}_{95}/\text{SiO}_2\text{-Al}_2\text{O}_3$	69.8	3.8	187 (191)	0.66 (0.67)	78 (79)	1.4 (1.4)
2 wt.% $\text{Pt}_5\text{Ir}_{95}/\text{H-SA}$	31.1	1.7	194 (85)	0.68 (0.30)	81 (35)	1.4 (3.1)
2 wt.% $\text{Pt}_5\text{Ir}_{95}/\text{ZrO}_2$	31.2	1.7	79 (85)	0.28 (0.30)	33 (35)	3.4 (3.1)
2 wt.% $\text{Pt}_5\text{Ir}_{95}/\text{MgO}$	13.4	0.7	23 (37)	0.08 (0.13)	10 (15)	11.5 (7.3)
2 wt.% $\text{Pt}_5\text{Ir}_{95}/\text{SiO}_2$	8.5	0.5	25 (23)	0.09 (0.08)	10 (10)	10.9 (11.5)
2 wt.% Ir/CeO_2	90.1	5.0	249 (248)	0.87 (0.87)	104 (103)	1.1 (1.1)
2 wt.% $\text{Pt}_5\text{Ir}_{95}/\text{CeO}_2$	95.5	5.2	332 (262)	1.17 (0.92)	138 (108)	0.8 (1.0)
2 wt.% $\text{Pt}_{15}\text{Ir}_{85}/\text{CeO}_2$	83.6	4.5	223 (226)	0.79 (0.81)	92 (94)	1.2 (1.2)
2 wt.% $\text{Pt}_{25}\text{Ir}_{75}/\text{CeO}_2$	80.9	4.3	225 (216)	0.81 (0.78)	93 (89)	1.2 (1.2)
2 wt.% $\text{Pt}_{50}\text{Ir}_{50}/\text{CeO}_2$	67.3	3.5	174 (174)	0.65 (0.65)	72 (71)	1.6 (1.6)
2 wt.% Pt/CeO_2	51.2	2.5	142 (124)	0.57 (0.50)	57 (50)	2.0 (2.2)

The TPR traces for the 2 wt.% Pt₅Ir₉₅/support catalysts presented in Fig. 3.9 c) display curve features of greater diversity. In general, and in fair agreement with XPS results (position of the Ir 4f_{7/2} line), all catalysts but the MgO-based are properly reduced when reaching 400 °C. Judging from its TPR trace, the MgO-based catalyst seems to have the noble metals buried inside the bulk structure. Except for the MgO-based catalyst and, the ceria and zirconia-based catalyst where hydrogen spillover is encountered, the other different-supported catalysts have one to two low-temperature peaks (< 250 °C) that may be attributed to reduction of noble metal species. Corresponding H₂ uptake values indicate fairly well a successful reduction process. For the H-SA-based catalyst, though, it is clear that the amount of deposited metals is too low and somehow the catalyst preparation failed.

In connection with the TPR analysis, dynamic CO pulse chemisorption was conducted. The catalysts have hence attained a previous reduction temperature of 500 °C. The results are presented in Table 3.4 and lists CO uptake value, metallic surface areas, CO/M ratio and dispersion and estimated average particle size. Surprisingly, the 2 wt.% Pt₂₅Ir₇₅/boehmite catalyst prepared from incipient wetness has a somewhat lower CO uptake value than its counterpart prepared from microemulsion. The CO uptake value is the starting point for all other properties calculated in Table 3.4. Taking into account the results from SEM and TEM, it seems rather peculiar that both catalysts have chemisorption properties of approximately the same magnitude. From quantitative TPR it is evident that with respect to the H-SA-based catalyst, the theoretical metal content value is to be trusted. In essence, the chemisorption properties of the various Pt₅Ir₉₅/support catalysts may be divided into four distinct groups: CeO₂ > γ-Al₂O₃, SiO₂-Al₂O₃ > H-SA, ZrO₂ > MgO, SiO₂. Due to the intrinsic CO uptake affinity shown by the ceria support itself, the CO uptake values for all ceria-based catalysts have been corrected to show the net value, hence attributed to the metal(s) only. It is clearly seen that as the relative loading of Pt increases, the chemisorption properties are progressively impaired. As previously mentioned, it is known that partially reduced surface ceria may cause metal decoration effects. In a HREM study of the nanostructural evolution of a Pt/CeO₂ catalyst during reduction, Bernal et al. [128] noted metal decoration effects upon reduction at 700 °C. After T_{red} ≤ 500 °C, however, the Pt microcrystals looked clean and well faceted. Since it seems very unlikely that one metal should be more decorated than the other, the explanation for the present deterioration must be found elsewhere.

Employing HREM and H₂ chemisorption, Zecua-Fernández et al. [100] obtained unequivocal results with respect to particle size of 1 wt.% Pt, Pt₈₀Ir₂₀, Pt₅₀Ir₅₀, Pt₂₀Ir₈₀ and

Ir (from aqueous solutions of H_2PtCl_6 and H_2IrCl_6) deposited on Al_2O_3 , TiO_2 and SiO_2 , final catalysts previously reduced at 500 °C. Upon introduction of Ir, the average particle size was progressively reduced. Alumina-based catalysts were shown to have nearly twice as good dispersion properties as silica-based catalysts with titania in between. Bulk analyses obtained from XRD on 4 and 8 wt.% silica-based catalysts showed that as the relative amount of Ir was increased from 0 to 100, the (3 1 1) reflection was linearly shifted from Pt to Ir and the unit cell parameter calculated applying Bragg's law was seen to decrease accordingly. This proved that the bimetallic phase is also of fcc type. In spite of this, no explanation was given of why the particle size changes.

The acid/base character of the catalysts was investigated by means of diffuse reflectance infrared fourier transform spectroscopy (DRIFTS). The spectra were taken after in-situ reduction at 400 °C and subsequent saturation with ammonia at 120 °C. A selection of

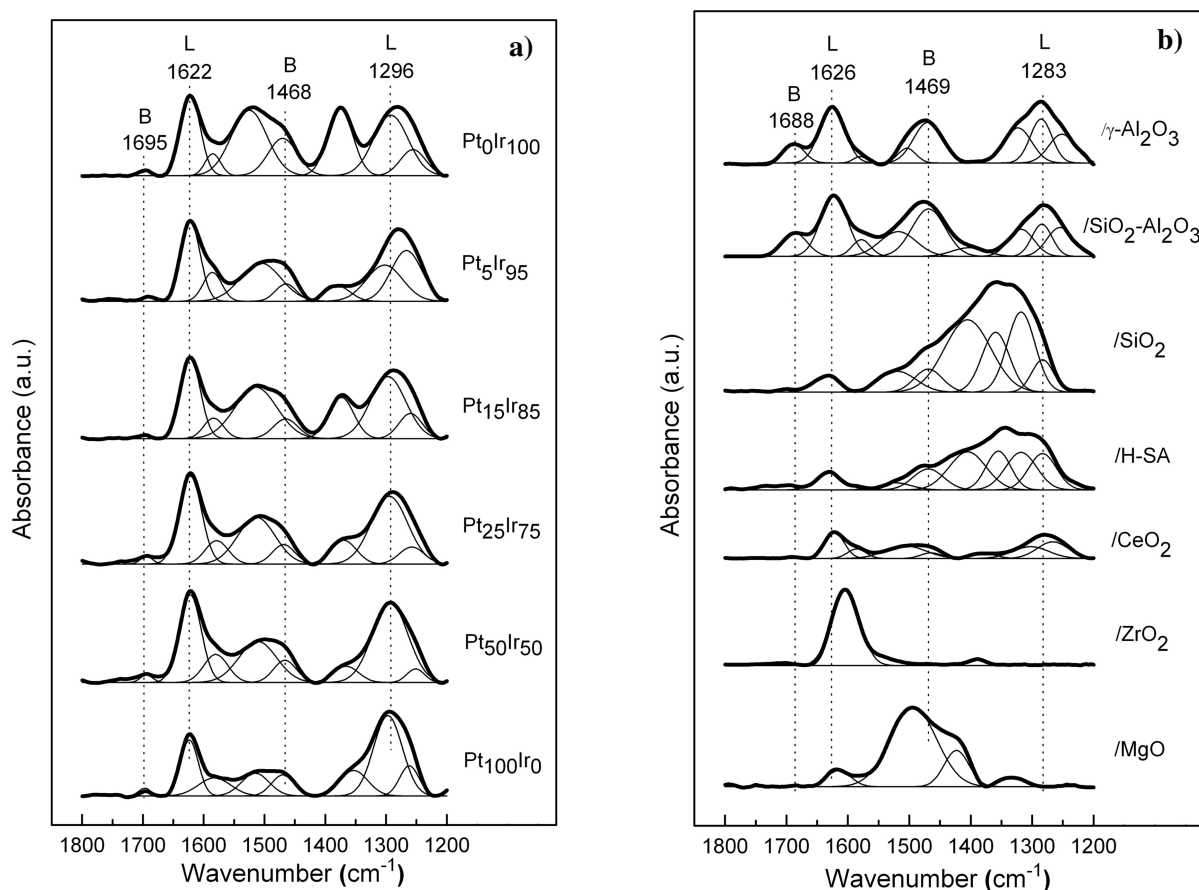


Figure 3.10 DRIFT spectra of chemisorbed NH_3 obtained at 120 °C on in-situ reduced (H_2 , 400 °C)

2 wt.% IW catalysts:

a) $\text{Pt}_x\text{Ir}_y/\text{CeO}_2$

b) $\text{Pt}_5\text{Ir}_{95}/\text{support}$

evaluated spectra is presented in Fig. 3.10. To the left, the ceria-based catalysts display very similar band features whereas, as expected, the Pt₅Ir₉₅/support catalysts have bands with quite diverse features. The spectra were fully peak deconvoluted in the 1200-1800 cm⁻¹ range employing Gaussian functions. The main objective was to locate the peaks commonly ascribed to Brønsted and Lewis acid sites: $\nu_{\text{as}}(\text{NH}_4^+) = 1455 \text{ cm}^{-1}$, $\nu_{\text{s}}(\text{NH}_4^+) = 1683 \text{ cm}^{-1}$ and $\nu_{\text{s}}(\text{NH}_3) = 1287 \text{ cm}^{-1}$, $\nu_{\text{as}}(\text{NH}_3) = 1614 \text{ cm}^{-1}$, respectively [131]. In Fig. 3.10, these four bands are emphasized but it is evident that the spectral patterns are far more complex as the nonlinear least squares fitted deconvolutions of the severely overlapping traces all contain up to nine individual curve components and peak maxima are found at eleven different positions. For example, the spectra of the SiO₂ and H-SA-based catalysts possess several intense and accentuated band features in the 1250-1550 cm⁻¹ range. Consequently, if neglecting these peaks in between the L_s and B_{as}, an estimation of acidity might be substantially underestimated. Moreover, the intense band observed for the magnesia-based catalyst at 1493 cm⁻¹ and that at 1604 cm⁻¹ observed for the zirconia-based catalyst are somewhat nebulous, although the latter may probably be attributed to L_{as} sites. The identification of the various peaks requires complementary quantitative techniques and is outside the scope of the present thesis. However, in order to have at least an idea about the relative acidity ranking between catalysts, a semi-quantitative evaluation based on the area of the 1470 cm⁻¹ B_{as} band was performed. With respect to ceria-based catalysts the trend is (arbitrary area values in brackets): Pt₀Ir₁₀₀(2.3) > Pt₅₀Ir₅₀(1.1) > Pt₁₅Ir₈₅, Pt₁₀₀Ir₀(1.0) > Pt₂₅Ir₇₅(0.9) > Pt₅Ir₉₅(0.8) and for Pt₅Ir₉₅/support catalysts: SiO₂-Al₂O₃(10.1) > γ -Al₂O₃(7.3) > SiO₂, H-SA (4.1) > CeO₂(0.8) > ZrO₂, MgO (0).

3.4.3 Miscellaneous characterization techniques employed

Worthwhile mentioning, a few other characterization techniques were utilized during the course of the present studies. These include FT-IR of adsorbed CO, Atomic Force Microscopy (AFM), X-ray Diffraction (XRD) and static volumetric H₂ chemisorption.

Results from FT-IR of adsorbed CO experiments are given in Paper IV but interpretation of the bands is not straightforward, in fact it may be questioned whether it is appropriate to assign a single CO-Ir stoichiometry factor for all catalysts as done in the evaluation of CO chemisorption data. The literature is rather incongruous, for example, the most prominent band at ca. 2075 cm⁻¹ has been ascribed to either Ir-carbonyl, Ir-dicarbonyl and even Ir-polycarbonyls species. However, the results from CO chemisorption are fairly well corroborated as the presence of two distinguishable bands in the 2000-2100 cm⁻¹

range seems indicative of highly dispersed surface Ir. An interesting observation is that for ceria-based catalysts, the high-frequency peak is clearly seen to shift towards higher frequencies for the bimetallics compared to the monometallics and it was tentatively proposed to be an additional proof of the achievement of alloying.

AFM is a relatively new, powerful technique that enables three-dimensional atomic resolution images of surface topography [132]. Briefly, the AFM analyses further corroborated the results from SEM and TEM with respect to the large metal agglomerates found for the Pt₂₅Ir₇₅/boehmite ME catalyst (additionally reduced at 450 °C).

Regarding XRD, besides bulk structure analysis it is possible to obtain information on the average particle size(s) by analysing specific diffraction line characteristics and employing the Scherrer equation. However, reliable data are only possible down to approximately 5 nm since smaller crystallites give lines that are too broad to be distinguished from the baseline [115]. Moreover the position of the peak(s) may reveal information about the metal intimacy in bimetallics. As the metal loading in the majority of the catalysts was only 2 wt.%, detector response intensities were too weak. Many attempts were made, but not even reducing the scan step angle and increasing the time per step resulted in useful spectra. A general remark is that for metal peaks to appear at least 4-5 wt.% is needed, moreover Al₂O₃ and TiO₂ supports cannot be used since their X-ray reflections will interfere with the Pt and Ir diffraction peaks [99,100].

H₂ chemisorption analyses performed in a static volumetric apparatus give the opportunity to obtain solely the amount of strongly chemisorbed probing molecules by subtracting the isotherm of the total uptake by that obtained after evacuation, the latter representing the weakly bound probing molecules. A number of the most interesting catalyst candidates were sent to an external partner who routinely performs such analyses. In general, results were severely divergent and the degree of dispersion was seen to differ between 15 to 70 % for a single sample why the results had to be rejected.

4 Catalytic behaviour

4.1 Ring opening of indan at atmospheric pressure

4.1.1 Catalyst pre-treatment

In the case of powdered catalysts, these had to be resized into pellets, crushed and sieved into the specific size fraction employed. This $120 < d_p < 250 \mu\text{m}$ particle size distribution was employed in all experiments and was initially chosen because the particles are large enough to avoid possible pressure drop over the bed and small enough to avoid internal mass transfer limitations. Prior to the catalytic experiments the catalysts were reduced in situ at either at 400 or 450 °C for one hour in excess hydrogen, i.e. ca. $100 \text{ cm}^3(\text{n})/\text{min}$, before the system was brought down to the reaction temperature 325 °C.

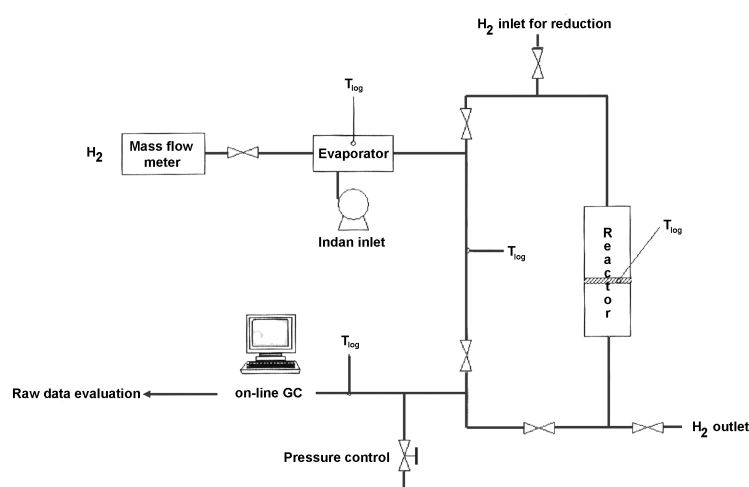


Figure 4.1 Schematic diagram of the catalytic screening apparatus operating at atmospheric pressure

Table 4.1 Typical experimental conditions employed when investigating the catalytic ring-opening reaction of indan

Reaction conditions	On-line product analysis by Varian 3800 GC-FID
Temperature: 325 °C	GC-program: 110 °C, 30 min (isothermally)
Reaction pressure: atmospheric	Capillary column CP-Sil 5 CB (50 m x 0.32 mm x 1.2 µm)
H ₂ /indan molar ratio: ~ 63	
Space velocities (τ): LHSV: 0.4-1.4 h ⁻¹ WHSV: 2.7 h ⁻¹ GHSV: 4500-17500 h ⁻¹	

4.1.2 Experimental apparatus and screening conditions

A continuous fixed bed catalytic reactor was used and it consists of an U-shaped glass tube with an inner diameter of 9 mm, encircled by an annular furnace. Liquid indan at a rate of 0.4 cm³/h was fed to an evaporator and then mixed with a carefully controlled stream of hydrogen (4.8 dm³(n)/h) yielding a H₂/indan molar ratio of 63. The obtained reaction mixture was subsequently directed over a standard weight 0.3 g catalytic bed placed on a porous disc inside the reactor. The schematic of the atmospheric pressure experimental apparatus is illustrated in Fig. 4.1. The activity test was carried out for 4.5 hr at 325 °C while every 30 minutes, the outgoing stream was analysed on-line by a Varian 3800 GC-FID (Gas Chromatography equipped with a Flame Ionization Detector). Chromatographic methods were elaborated to analyse the reaction products in the MCP, indan and tetralin ring-opening reactions. Reaction parameter settings or corresponding ranges utilized in the catalytic experiments with indan and details on the analytical product evaluation procedure are summarised in Table 4.1.

4.1.3 Catalytic results

A typical well-resolved chromatogram obtained when screening a 2 wt.% Pt-Ir-based catalyst with indan is presented in Fig. 4.2. The identification of reaction compounds, those in liquid form at ambient temperature and pressure, was preliminarily conducted by comparing the retention times with respect to indan in the reaction chromatogram with corresponding retention times in chromatograms obtained for pure reference compounds. The attribution of these peaks has been confirmed by mass spectrometry analysis. The desired reaction products, as evidenced in Fig. 2.2, are 2-ethyltoluene and

n-propylbenzene where the naphthenic ring has been cleaved only once leaving the molecular weight almost unaffected. Of these two, *n*-propylbenzene is most desired as the cetane number is positively affected by less branching. In agreement with previous results reported in the literature for catalytic ring opening of indan, endocyclic scission of the naphthenic C₅ ring at the unsubstituted (β) C-C bond is strongly favoured as evidenced by the considerably larger quantity of 2-ethyltoluene formed [78-81]. However, in the absence of a catalyst during thermal (460 – 540 °C) high-pressure (10 – 160 atm) hydrogenolysis of indan, Penninger and Slotboom [133] noted conversely the preference for endocyclic cleavage at the substituted (α) C-C bond. From a cetane and liquid yield point of view, further dealkylation is highly undesired and results in *o*-xylene, ethylbenzene, toluene, benzene and lights (<C₆).

After the reactor, the out-going reaction stream was maintained above the boiling point of indan in order to avoid condensation and the effluent stream entered the gas chromatograph as a single hydrocarbon mixture.

The FID detector responds roughly to the number of carbon atoms entering per unit of time, i.e. it is a mass-sensitive analyser [134]. Due to the lack of an on-line mass spectrometer, only the major C₆-C₉ constituents were identified and as seen in Fig. 4.2, hydrocarbons with less than six carbon atoms were generically termed “lights”. Consequently, selectivity could not be reported on a molar basis but was given on mass

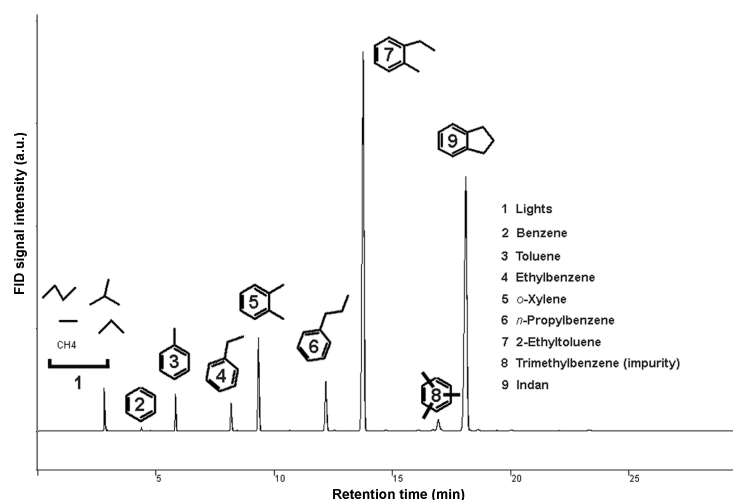


Figure 4.2 A typical GC-FID chromatogram obtained when indan is catalytically converted in the presence of hydrogen over a 2 wt.% Pt-Ir-based ring-opening catalyst at 325 °C and atmospheric pressure.

basis. For the sake of congruity, conversion was then given on mass basis as well. Although all products would have been identified, an exact analytical analysis requires the employment of response factors and for some reaction products these could be very difficult to establish, e.g. relating high boiling-point hydrocarbons such as indan (bp 176 °C) and gaseous hydrocarbons such as ethane. Due to these analytical limitations, no in-depth insights on reaction mechanisms have been obtained. In addition, it has to be emphasized that the principal objective of the RESCATS project was to come up with highly efficient catalysts ready for industrial implementation and that within a limited period of time. Consequently, and in agreement with the project plan, the scheduled research had to be strictly of applied nature and focused on catalyst synthesis, characterization and screening.

During the course of the present studies 55 different catalysts were synthesized and screened for ring-opening activity with indan, see section 3.3. In Fig. 4.3 and 4.4 the catalytic results for the 2 wt.% Pt₂₅Ir₇₅/boehmite catalysts prepared from microemulsion and incipient wetness are shown.

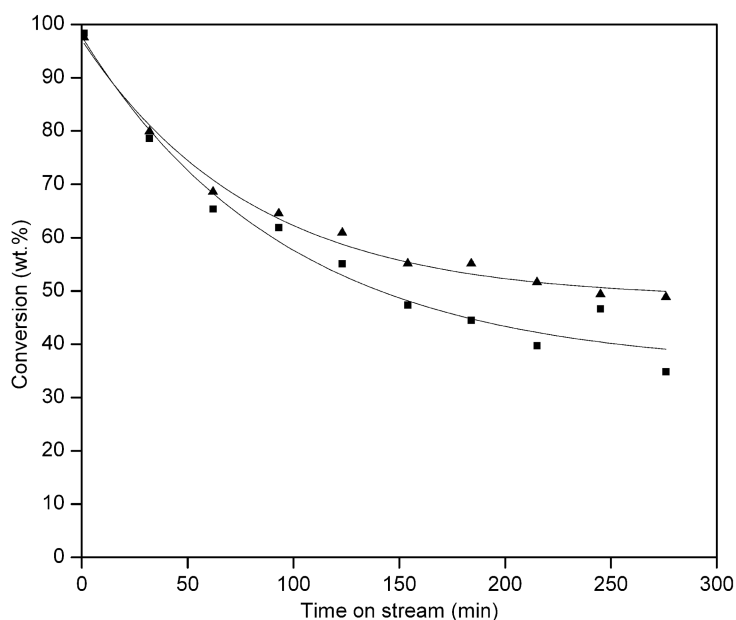


Figure 4.3 Activity test with indan at atmospheric pressure and a temperature of 325 °C over 2 wt.% Pt₂₅Ir₇₅/boehmite catalysts prepared from different techniques: incipient wetness (▲); microemulsion (■).

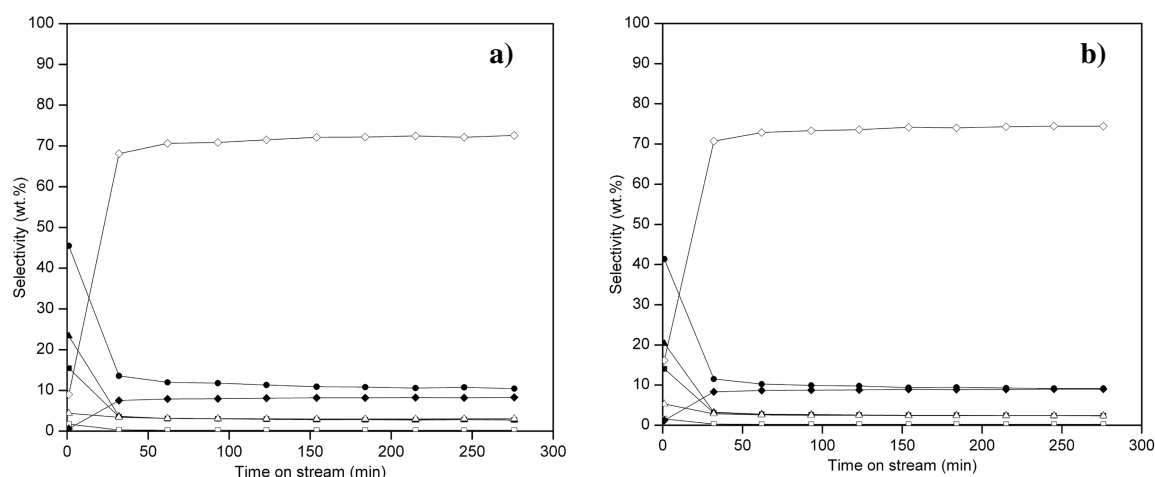


Figure 4.4 Product selectivity (wt.%) observed in the reactions presented in Fig. 4.3. Lights (■), benzene (□), toluene (▲), ethylbenzene (Δ), *o*-xylene (●), *n*-propylbenzene (◆), 2-ethyltoluene (◇):

a) the microemulsion catalyst

b) the incipient wetness catalyst

With respect to conversion of indan versus time-on-stream both catalysts initially display a very high activity, reaching almost 100 %, but then the conversion progressively declines following an exponentially decaying function. It is evident that the IW catalyst has the better performance. In Fig. 4.4, it is seen that the two catalysts display very similar selectivity values during the reaction. However, small variations may be observed, in particular with respect to the first experimental point acquired after one minute on stream, when exposing the in-situ reduced catalyst surfaces to the indan/hydrogen reactant mixture. Already after the second data point (after slightly more than 30 minutes on stream), the product selectivity starts to level out and reaches a steady state. Apparently, some dramatic restructuring of the virgin surfaces must occur initially as evidenced by the remarkable transformation in product selectivity between the first and the second data point. In essence, the incipient wetness catalyst displays less cracking activity, which may be seen by the initially lower selectivity values for *o*-xylene, toluene and lights and higher selectivity for the desired 2-ethyltoluene. Subsequently, during the course of the screening test, the principal difference observed is the higher selectivity for 2-ethyltoluene and lower selectivity for *o*-xylene witnessed over the IW catalyst.

Although the dynamic CO chemisorption results showed a slightly higher CO uptake value for the ME catalyst and hence indicated a somewhat more dispersed metals phase containing on average smaller particles, the catalytic data are better explained in view of

the findings from TEM. In fact, the higher cracking activity and lower indan conversion level observed for the ME catalyst is due to a less homogeneous bimetallic phase. Fig. 4.5

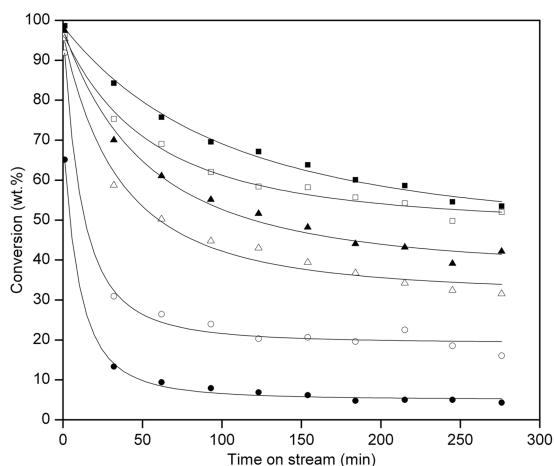


Figure 4.5 Activity test with indan at atmospheric pressure and 325 °C over the 2 wt.% Ir (■), Pt₅Ir₉₅ (□), Pt₁₅Ir₈₅ (▲), Pt₂₅Ir₇₅ (Δ), Pt₅₀Ir₅₀ (○) and Pt (●)/CeO₂ catalysts.

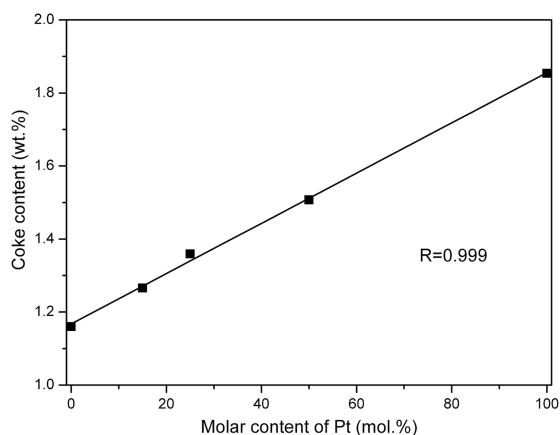


Figure 4.6 Results from the TPO-TG-MS experiments showing the amount of deposited coke in the spent 2 wt.% Pt_xIr_y/CeO₂ catalysts vs. the molar content of Pt.

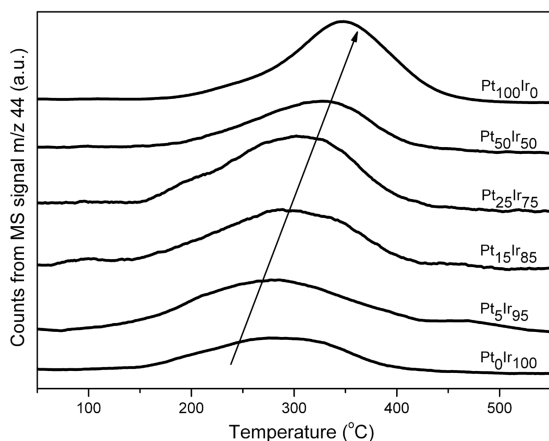


Figure 4.7 Coke distribution in the spent 2 wt.% Pt_xIr_y/CeO₂ catalysts visualized by the m/z 44 (CO₂) signal acquired during TPO-TG-MS.

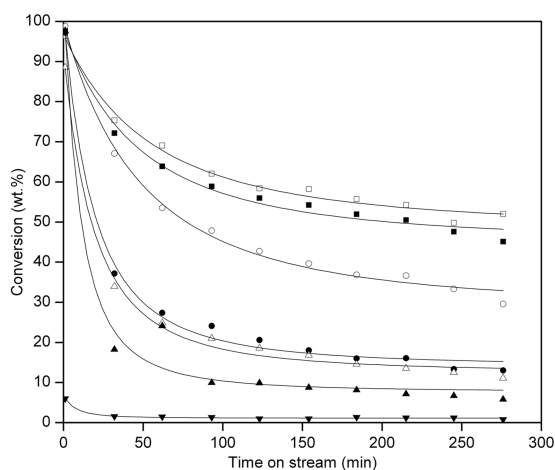


Figure 4.8 Activity test with indan at atmospheric pressure and 325 °C over 2 wt.% Pt₅Ir₉₅/supported catalysts: CeO₂ (□), γ-Al₂O₃ (■), SiO₂-Al₂O₃ (○), H-SA (●), ZrO₂ (Δ), MgO (▲) and SiO₂ (▼).

shows the activity curves obtained for the 2 wt.% Pt_xIr_y/CeO₂ catalysts prepared from incipient wetness. It clearly shows that as the amount of iridium is increased, the activity curve is shifted upwards. From CO chemisorption data and quantitative XPS results it is evident that the decisive parameter is the surface accessibility of Ir. The activity trend with monometallic Pt catalysts exhibiting the lowest level of hydrogenolysis activity, monometallic Ir the highest and bimetallics in intermediate positions has been observed by several researchers in the case of, for example, propane [135] and hexane hydrogenolysis [100,136]. This is not only because Ir has an intrinsically higher hydrogenolysis activity than that of Pt, for example visualized in the present study at the first experimental point in Fig. 4.5 with respect to indan conversion and selectivity to lights (Paper III, Table 4), but also due to its hydrogenation properties that allows for coke precursor annihilation. From reforming studies it is known that the addition of Ir to Pt/Al₂O₃ catalysts lowers the rate of coke deposition [88,89,102]. Indeed, coke analysis of the spent ceria-based catalysts by means of TPO-TG-MS, presented in Fig. 4.6, reveals a perfectly linear relationship between the amount of deposited coke and the amount of Pt in the catalyst. Concomitantly, it may be observed in Fig. 4.7 that the position of the m/z 44 peak attributed to CO₂ is seen to shift towards higher temperatures indicating a more dehydrogenated character of the deposited coke, however, still residing on the metal phase [137]. For the various-supported Pt₅Ir₉₅ catalysts presented in Fig. 4.8, the level of indan conversion represented by the vertical curve position is clearly seen to correlate with CO chemisorption data, see Table 3.4. Moreover, for these catalysts, except the zirconia-based, the amount of deposited coke agrees with the Brønsted acidity trend, semi-quantitatively estimated from NH₃-DRIFTS. According Barbier et al. [137], support acidity-induced coke should manifest itself in a peak at approximately 450 °C with respect to the m/z 44 signal in the TPO-TG-MS spectrum, however, such a high-temperature peak was not experimentally observed for the most acidic catalysts (based on γ-Al₂O₃ and SiO₂-Al₂O₃).

In conclusion, catalyst acidity indeed promotes coking but the atmospheric pressure ring-opening reaction is metals driven and the conversion of indan is chiefly governed by the accessibility of surface Ir. Selectivity values obtained from the different catalysts have not differed significantly with respect to desired products. Taking into account all screened catalysts, the steady state selectivity value is in the range 60-80 wt.% for 2-ethyltoluene and approximately 10 wt.% for *n*-propylbenzene. Although no systematic investigation of the influence of particle size on catalytic performance has been conducted, it seems as if the reaction is structure insensitive (e.g. comparing the 2 wt.% Pt₂₅Ir₇₅/boehmite catalyst prepared from microemulsion and incipient wetness, respectively).

4.2 Evaluation of the best catalyst candidate with the real feed HDT-LCO

During the course of the RESCATS project 19 catalyst candidates in total were evaluated at the two refinery partners in their pilot units under industrially employed conditions, i.e. high pressure (40 bar). The catalysts were initially screened with one or two model feed mixtures (i.e. indan or tetralin in n -C₁₄ or n -C₁₆) and then subjected to the HDT-LCO real feed.

Out of these 19 catalyst candidates, the most promising emerged from the present work: the 2 wt.% Pt₅Ir₉₅/CeO₂ catalyst prepared from incipient wetness, henceforth abbreviated KTH-3 (Paper V). It is outside the scope of the present thesis to analyse the high-pressure evaluation activities in detail but as the author conducted a re-evaluation of KTH-3 at CEPESA, the most significant results with respect to HDT-LCO upgrading will be presented.

4.2.1 Experimental apparatus, catalyst pre-treatment and experimental conditions

The initial catalyst pellets ($0.12 < d_p < 0.25$ mm) were crushed, pelletized, then carefully crushed and sieved into a $0.84 < d_p < 1.14$ mm size fraction, in total 20 cm³. The catalyst was physically mixed 1:1 on volume basis with $0.4 < d_p < 0.6$ mm glass beads (SiC) and loaded into the steel cylinder of the fixed bed micro pilot plant. Prior to the catalytic experiment the catalyst was activated by in-situ reduction employing 15 dm³(n)/h hydrogen at atmospheric pressure and the following temperature ramp: $T_{\text{room}} \rightarrow 300$ °C (2 °C/min), dwell 3 hr, $300 \rightarrow 450$ °C (2 °C/min), dwell 1 hr. Operating parameters for

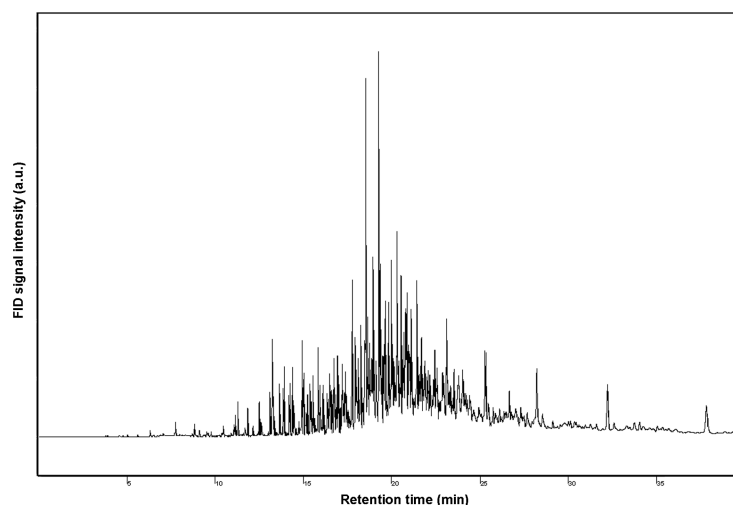


Figure 4.9 GC-FID chromatogram obtained from the HDT-LCO feed

Table 4.2 Characteristics of the HDT-LCO fraction for high-pressure evaluation at CEPESA

Physical/chemical property	Value
Aromatics distribution (wt.%)	
Monoaromatics	53.1
Diaromatics	10.9
Tri+ aromatics	3.9
Total	67.9
Sulphur (ppm(wt))	40
Nitrogen (ppm(wt))	111
Density (kg/dm ³)	0.9023
Cetane index	31.4
Distillation ASTM-D86 (°C)	
10 vol.%	221.5
30 vol.%	246.5
50 vol.%	263.0
70 vol.%	288.5
90 vol.%	326.5

pilot testing were set to match the operating conditions of a commercial unit under industrial running. These were: 40 bar (over)pressure, LHSV=1.0 h⁻¹, H₂/HC ratio=750 dm³(n)/dm³. The effect of reaction temperature, expressed as the weighted average bed temperature (WABT), was investigated in the range from 200 to 360 °C.

The HDT-LCO stream is a complex petroleum fraction consisting of hundreds of individual hydrocarbon species. The GC-FID chromatogram of the particular HDT-LCO feed utilized by CEPESA is presented in Fig. 4.9. It clearly illustrates that product evaluation is preferably conducted taking into account the sample as a whole, or at least dividing the constituents into groups and subgroups.

Consequently, in the product evaluation from processing HDT-LCO over the ring-opening catalyst, standardized test methods were employed including the aromatic distribution (EN 12916), density (ASTM D4052-96), total sulphur (ASTM D5453-03a), total nitrogen (ASTM D4629-02), average boiling point (calculated on the basis of the results obtained from ASTM D86-03) and cetane index (ASTM D4737-03). Important characteristics of the HDT-LCO feed are enumerated in Table 4.2.

4.2.2 Catalytic results

The variation in key diesel fuel properties as a function of reaction temperature (WABT) is shown in Figs. 4.10-4.13. In general, the catalyst (KTH-3) is characterized by a very

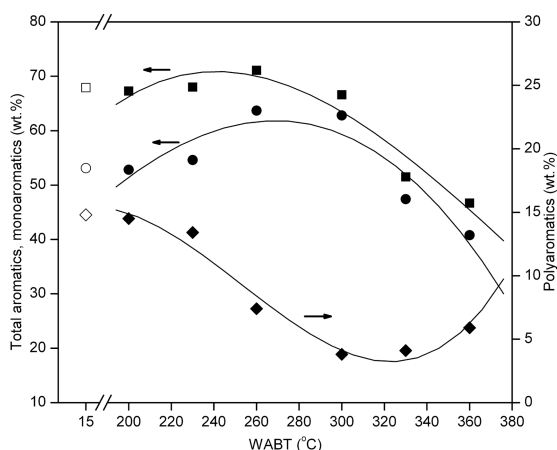


Figure 4.10 The distribution of aromatics as a function of reaction temperature when processing the HDT-LCO over the 2 wt.% $\text{Pt}_5\text{Ir}_{95}/\text{CeO}_2$ catalyst: total aromatics (■), monoaromatics (●), polyaromatics (◆), HDT-LCO feed values (□, ○, ◇, respectively).

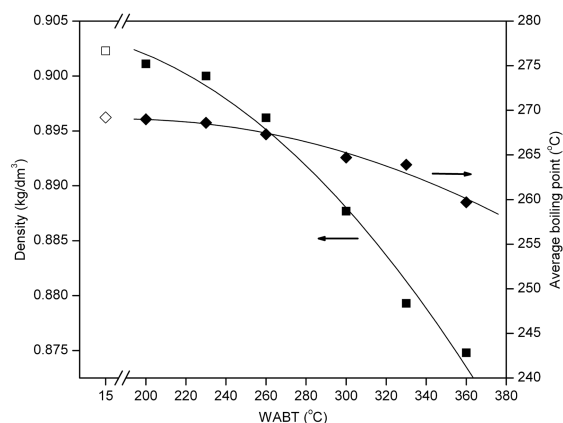


Figure 4.11 Variation in product density and product average boiling point as a function of reaction temperature when processing the HDT-LCO over the 2 wt.% $\text{Pt}_5\text{Ir}_{95}/\text{CeO}_2$ catalyst: density (■), average boiling point (◆), HDT-LCO feed values (□, ◇, respectively).

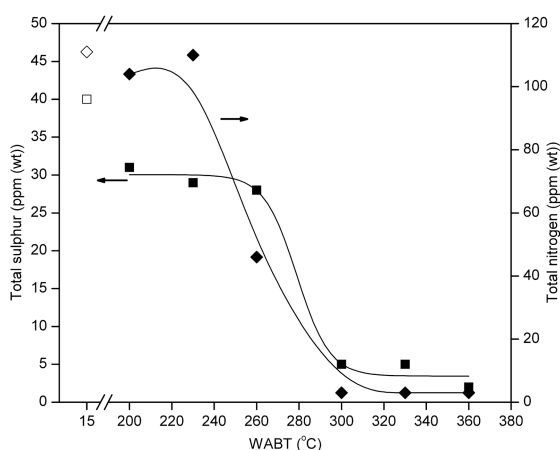


Figure 4.12 Variation in product sulphur and nitrogen content as a function of reaction temperature when processing the HDT-LCO over the 2 wt.% $\text{Pt}_5\text{Ir}_{95}/\text{CeO}_2$ catalyst: total sulphur (■), total nitrogen (◆), HDT-LCO feed values (□, ◇, respectively).

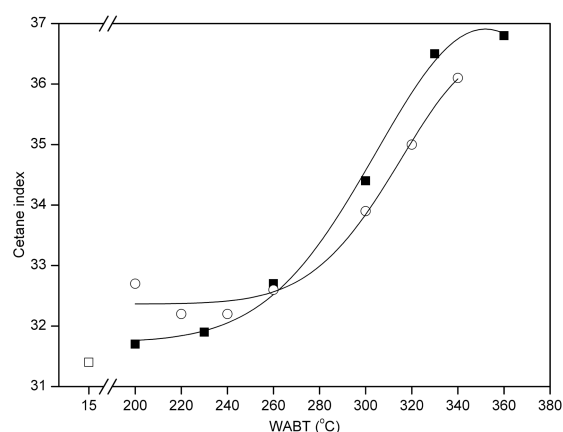


Figure 4.13 Variation in cetane index as a function of reaction temperature when processing the HDT-LCO over: the 2 wt.% $\text{Pt}_5\text{Ir}_{95}/\text{CeO}_2$ catalyst (■), a commercial catalyst (○), HDT-LCO feed value (□).

high activity with respect to performance in reducing level of aromatics, density, average boiling point, sulphur and nitrogen contents and in improving the cetane index. The overall product quality is enhanced when increasing the reaction temperature. The distribution of aromatics (mono, poly and total) detailed in Fig. 4.10 evidences that the catalyst has good hydrogenation properties with decreasing content of mono and total aromatics versus temperature. The amount of polyaromatics is well below the imposed 11 wt.% limit as the temperature exceeds 240 °C. In line with the information provided in Fig. 2.1 on aromatics-hydrogenation thermodynamics, the test unit should not be operated at temperatures above 380 °C in order to avoid dehydrogenation. Moreover, at such high temperatures consecutive cracking reactions beyond ring opening result in unacceptable liquid yield losses. In addition, at such high temperatures also cracking due to thermolysis must be accounted for.

Fig. 4.11 shows the results with respect to density and average boiling point. Although a substantial improvement is reached from the starting 0.9023 kg/dm³, the density value of 0.845 kg/dm³ imposed by present legislation is never met. The reduction in density may also be reflected in the declining average boiling point curve.

The removal of the heteroatoms sulphur and nitrogen is, as shown in Fig. 4.12, readily achieved in the temperature range investigated. With respect to nitrogen removal, there is more or less no activity observed until 240 °C from which the nitrogen content markedly drops down to a level below 5 ppm (wt) at 300 °C. The reduction of sulphur displays similar characteristics: at 300 °C the sulphur content is down to below 5 ppm(wt) that by relatively wide margins meets the target EU specification set out for 2009 [35]. Some important aspects of hydrodesulphurization, including reaction mechanisms are discussed in section 5.1.

At last the most relevant diesel fuel property related to the present research work; that is the variation in cetane index (CI) as a function of reaction temperature reported in Fig. 4.13. The results are presented together with those obtained from a commercial diesel-quality improvement catalyst. The calculation for each data point is based on specific values acquired from the simulated-distillation curve and the density. The empirical equation has the following appearance [138]:

$$CI = 45.2 + (0.0892)(T_{10N}) + [0.131 + (0.901)(B)][T_{50N}] + [0.0523 - (0.420)(B)][T_{90N}] + [0.00049][(T_{10N})^2 - (T_{90N})^2] + (107)(B) + (60)(B)^2$$

D = density at 15 °C, g/mL determined by Test Methods D 1298 or D 4052

DN = D-0.85

B = [e^{(-3.5)(DN)}]-1

T₁₀ = 10 % recovery temperature, °C, determined by Test Method D 86 and corrected to standard barometric pressure

T_{10N} = T₁₀-215

T₅₀ = 50 % recovery temperature, °C, determined by Test Method D 86 and corrected to standard barometric pressure

T_{50N} = T₅₀-260

T₉₀ = 90 % recovery temperature, °C, determined by Test Method D 86 and corrected to standard barometric pressure

T_{90N} = T₉₀-310

It is clearly seen that the newly developed KTH-3 catalyst possesses superior cetane index boosting properties in comparison with the commercial counterpart. The improvement with respect to the HDT-LCO feed is a ΔCI of +5.4 points or +17 % at 360 °C. Although no mass balance closure was established, the corresponding GC-FID chromatogram presents only a few minor peaks within the first five minutes after injection. This is a reliable indication of the catalyst not giving rise to extensive cracking and thus the liquid yield losses may be assumed negligible. In Fig. 4.13 it is not possible to discern the specific contribution from aromatics saturation from that of ring opening upon the cetane index improvement. Yet, in Paper III, results from evaluating the KTH-3 catalyst at the other refiner (Saras) employing a different HDT-LCO cut containing considerably less aromatic species, similar cetane boosting characteristics were observed. By means of an in-house developed analytical procedure based on an extension of the EN 12916 method [139], refinery employees concluded that the catalyst at 320 °C produces a ring-opening yield of 3 wt.% in both the HDT-LCO upgrading reaction and the model feed reaction. At the end of the test with the HDT-LCO, they brought the system back to the first experimental conditions evaluated with this feed and noted a slight decrease of catalytic performance and attributed it to sulphur poisoning. However, during the evaluation of KTH-3 at CEPSA, upon introduction of the model feed after processing the

HDT-LCO, the catalyst was seen to fully regain its initial activity. Hence, the sulphur poisoning seems to be a reversible process.

In essence, in view of the above results and the realisation and registration of a first-to-invent official document (Paper **V**) in Spain and France promoted by industrial partners (CEPSA, CTI), the KTH-3 catalyst certainly has the potential of industrial implementation.

5 Sulphur in petroleum streams

As mentioned earlier sulphur itself has an inherently positive, lubricating effect on engine mechanics and reduces wear. For the environment, however, sulphur is hazardous. When organic sulphur compounds are combusted in engines, sulphur oxides are inevitably formed and contribute to both local and regional acidification. Moreover, sulphur is poisonous for noble metal-based catalytic exhaust gas clean-up systems (de-NO_x, CO and HC oxidation) and severely impairs the performance of such three-way catalysts. Pushed by gradually tightening environmental legislation specifications, the focus in the oil refining industry today is mainly set on lowering sulphur levels [27,36,37]. Fig. 5.1 shows how the maximum sulphur level allowed in European diesel fuel has decreased during recent years. The research for catalysts and accompanying process technologies that are capable of producing ultra-low sulphur diesel (ULSD), i.e. containing less than 10 ppm(wt) sulphur, is consequently a hot topic [22,140-144].

5.1 The need for sulphur characterization when refining petroleum

It is of utmost importance for catalyst manufacturers and petroleum refiners to be able to monitor the evolution of the sulphur distribution throughout the whole refining process, from well to final product. In general, the presence of certain sulphur compounds such as alkyl-substituted dibenzothiophenes (DBT) is more important than sulphur content alone. With target sulphur species identified, laboratory experiments can be more focused on elucidating reaction kinetics and mechanisms for these specific compounds and hence catalyst properties and reaction conditions can be optimised. It has long been recognized that in the case of hydrodesulphurization (HDS) of middle distillates and heavier streams such as gas oils, polyalkylated DBTs, in particular with alkyl substituents in the 4- and/or 6-positions next to the sulphur atom, are highly unreactive and difficult to remove [145,146]. HDS proceeds via two parallel reaction pathways; the dominating reaction will depend on the nature of the sulphur compound, the catalyst used and the reaction conditions employed. In the hydrogenolysis route the sulphur atom is directly removed from the molecule whereas for the hydrogenation route, the aromatic ring is first hydrogenated before removal of the sulphur atom. Typical HDS catalysts include

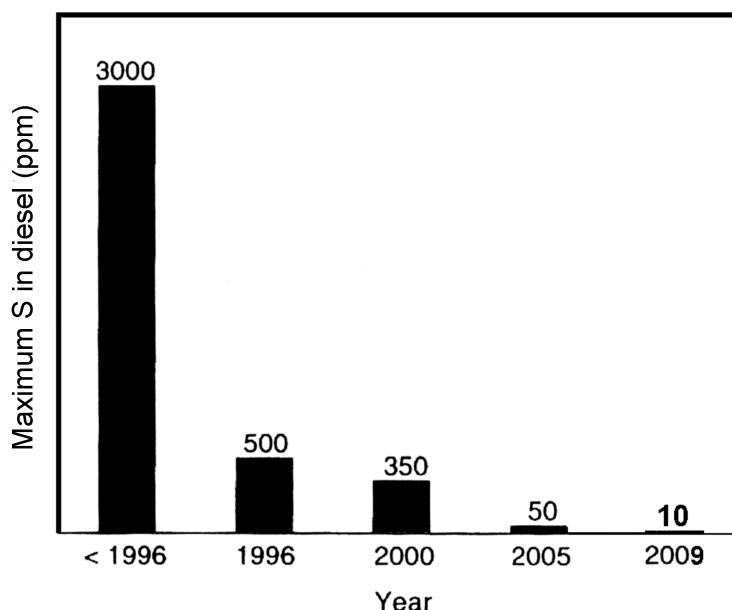


Figure 5.1 The development of sulphur level specification in European diesel fuel during the last years

sulphided Ni-Mo and Co-Mo as active components; the former brings the reaction forward preferably via the hydrogenation pathway whereas the latter is used where direct hydrogenolysis is sought for [22]. If the sulphur level is low enough noble metal-based catalysts might be considered, mainly for the reason that lower operating temperatures are required to obtain a given conversion [42]. For the noble metal-based ring-opening catalysts employed in this study, in order to optimize the activity, the sulphur distribution and amount in the HDT-LCO feed must be closely checked. In fact, one of the fundamental work packages in the RESCATS project was devoted to sulphur characterization of different feeds, intermediate streams and final products.

5.2 Analytical determination of sulphur compounds

Sulphur compounds are inherently difficult to measure because they are polar, reactive and rather often present at trace levels. This behaviour places stringent demands on sampling and analysis systems.

The analysis of sulphur distribution is normally conducted using high-resolution chromatography linked to a sulphur-specific detector. There are several detectors available on the market, for example the Flame Photometric Detector (FPD), the Hall Electrolytic Detector (HECD) and the Atomic Emission Detector (AED). The most powerful of them is perhaps the Sulphur Chemiluminescence Detector (SCD), invented in

the late 1980s by Stedman and Benner [147]. There are surprisingly few instruments to be found in Europe and it is most likely due to the fact that operating the instrument calls for careful maintenance and genuine know-how. Consequently, it might not be the first hand choice for on-line analysis but a recommendable alternative for separate high-quality analyses of complex petroleum samples. The detector is extremely sensitive and it is possible to detect individual sulphur species down to approximately 10 ppb! The general outline of the GC-SCD system is shown in Fig. 5.2. There are several advantages with the SCD in comparison with the other detectors mentioned earlier in the text. First of all the selectivity over carbon is very high and the absence of hydrocarbon interference results in clear sulphur chromatograms. Moreover, it has an almost perfectly equimolar and linear sulphur response over a wide range of concentrations implying that no external standards are necessary; adding one, carefully chosen, internal standard of known concentration is enough for quantitative measurements of the whole sulphur distribution and for determination of total sulphur content. Another attractive feature is that it is possible to obtain sulphur and hydrocarbon chromatograms simultaneously by using FID-SCD detectors in parallel or in series.

The principle of SCD operation is that organic sulphur compounds are first oxidised in a burner at 800 °C into sulphur monoxide that secondly reacts with ozone in a vacuum cell into sulphur dioxide. In the second reaction photons in the 300-400 nm range are emitted and these are detected and amplified in a photo multiplier tube (PMT) and the resulting

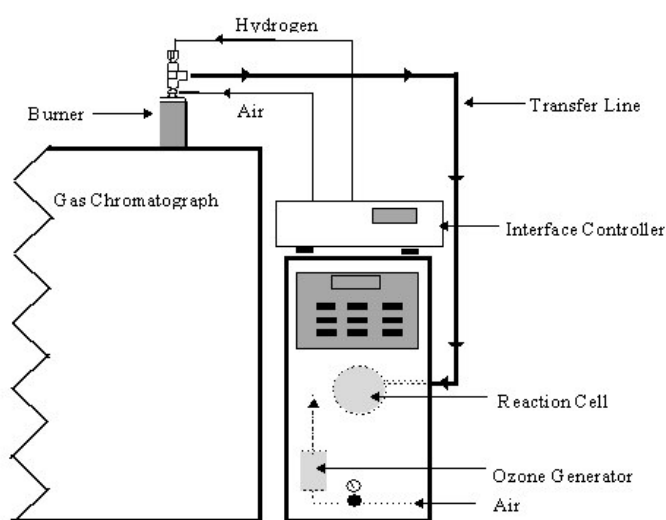
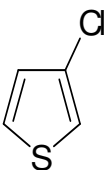
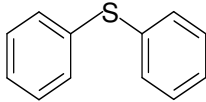
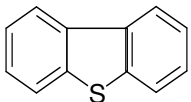


Figure 5.2 Schematic of the GC-SCD equipment

signal is used for realising a chromatogram. Further details on SCD theory and operation are found elsewhere [148,149].

At the division of Chemical Technology, KTH, there was an existing system configuration made up of a Hewlett-Packard GC model 6890 coupled to a Sievers SCD 355 detector. The instrument was successfully started up and the integrity and accuracy of the instrument were checked at an early stage by comparing various qualitative and quantitative results with corresponding information obtained at the two refineries using other techniques such as FPD and AED. A large number of analyses on different industrially relevant petroleum samples has been performed.

Table 5.1 Analysis conditions employed for GC-SCD analysis of sulphur in petroleum streams

Conditions	Type of sample	
	Lighter fraction	Heavier fraction
Column	SPB-1 Sulfur (30 m x 0.32 mm x 4 µm)	Equity-1 (30 m x 0.32 mm x 0.4 µm)
Internal standard	 3-Chlorothiophene	 Diphenylsulfide  Dibenzothiophene
<u>GC method</u>		
T _{ramp} oven:	35 °C hold 0.2 min 35 °C to 70 °C; 10 °C/min 70 °C to 280 °C; 3 °C/min	80 °C hold 3 min 80 °C to 120 °C; 5 °C/min hold 5 min 120 °C to 210 °C; 10 °C/min hold 5 min
Constant flow mode: 1.8 cm ³ /min (31 cm/s)		
Injector temperature: 300 °C		
Injection amount: 1 µl, split 4:1 / splitless		

5.3 Analysis conditions

Depending on the properties of the sample, whether it is a light (naphtha) or a heavy fraction (LCO, HDT-LCO), two specific methods have been carefully elaborated and used in order to obtain maximum chromatographic resolution. The analysis conditions are summarised in Table 5.1.

5.4 Results

Typical sulphur chromatograms of LCO and HDT-LCO are presented in Fig. 5.3. Prior to

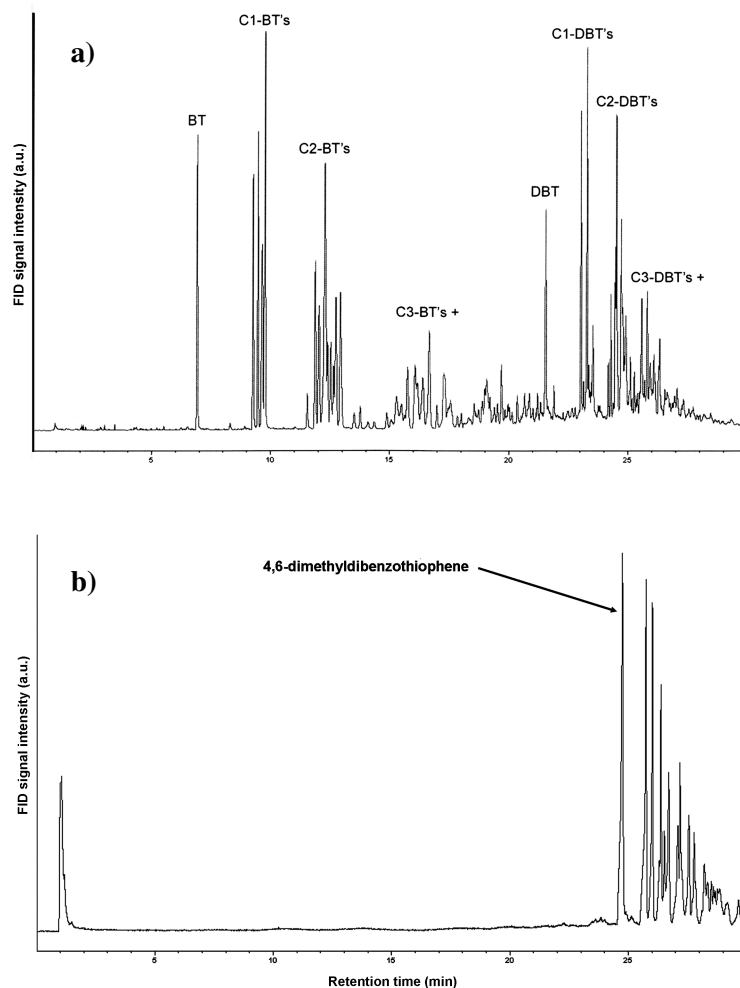


Figure 5.3 GC-SCD chromatograms of:

- a) LCO containing ~ 78 ppm(wt) S
- b) pure HDT-LCO ~ 40 ppm(wt) S

injection, the LCO sample was diluted in *n*-octane a hundred times to obtain approximately 78 ppm(wt) total sulphur. The peaks in the LCO chromatogram mainly originate from alkylated (mono, di and tri-) benzo and dibenzothiophenes, respectively. Positive identification and quantification were achieved for 29 individual aromatic sulphur compounds in the LCO (Paper VI). The identification was based on comparisons of relative retention times obtained with single reference compounds and the internal standard diphenylsulfide and corresponding time intervals in the spiked LCO sample. Quantitative analysis was conducted by adding an aliquot of the internal standard with known concentration to the diluted LCO sample, whereupon LCO peaks in the obtained chromatogram were all correlated to the area of the internal standard. The sulphur distribution is markedly shifted towards the heaviest classes, which is associated with the origin of the LCO, coming from hydrotreated vacuum gas oil. Due to the lack of commercially available reference substances of heavier polyalkylated dibenzothiophenes in the C3-DBT+ family, only one peak in the HDT-LCO chromatogram was identified; the 4,6-dimethyldibenzothiophene, known from the literature to be a particularly difficult compound to remove due to the steric hindrance by the methyl substituents in the close vicinity of the sulphur atom.

Fig. 5.4. displays the sulphur distribution in three different naphtha cuts, i.e. with different boiling point ranges. Typical sulphur compounds found in naphthas, derived directly from the atmospheric distillation unit, mainly include thiols, sulfides and thiophenes. The sulphur species that were identified in the various cuts are listed in the corresponding chromatogram. Since the compound identification is based on the use of single reference compounds the process is slow and could be much more effective if a mass-selective detector were employed. However, for identification of heavier alkylated aromatic sulphur molecules, where the number of isomers increases drastically with the degree of alkylation, a mass-selective detector would not be as useful.

When the ring-opening catalyst candidates were evaluated in the pilot units at the refineries using real feed HDT-LCO, the product stream was periodically sampled at different reactor temperatures and subsequently characterized for sulphur content and distribution. As expected the total sulphur content decreased with increasing operating temperature but the relative sulphur distribution did not markedly change. When the sulphur content in these particular petroleum streams got below approximately 10 ppm(wt) hardly any peaks could be discriminated from the baseline although increasing injection volumes and operating in splitless mode.

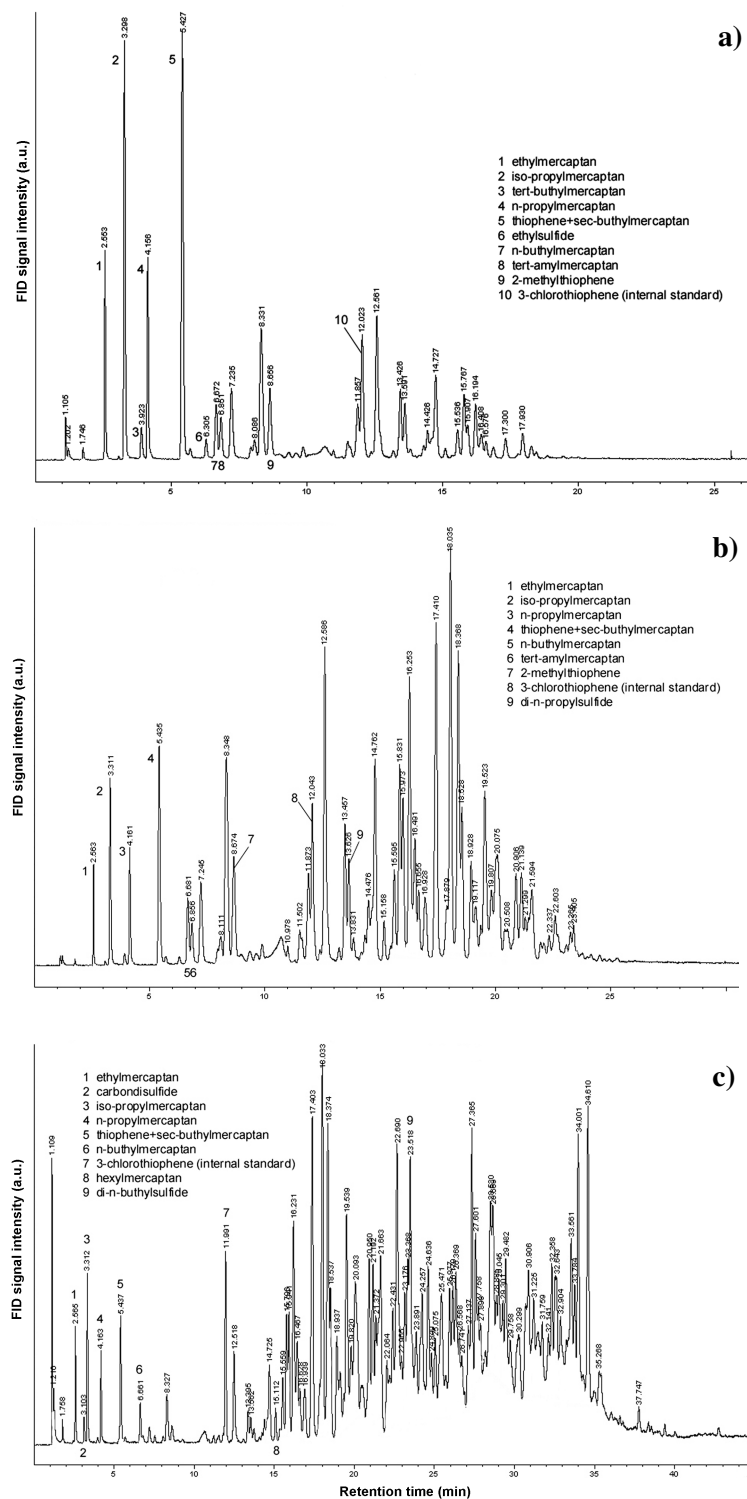


Figure 5.4 GC-SCD chromatograms of various naphtha cuts including identified sulphur compounds

a) C5-149

b) 95-175

c) 149-232

Table 5.2 An assortment of quantitative GC-SCD results obtained at KTH compared to results obtained at the refineries in the RESCATS project. KTH-2 and KTH-3 are pilot unit 2 wt.% Pt₅Ir₉₅/support ring-opening catalysts

Sample	Internal standard	KTH results (ppm(wt)) ^a	Refinery results (ppm(wt))	Difference (%)
LCO	Diphenylsulfide	7865	7751 ^b	+1.5
HDT-LCO	Dibenzothiophene	33	40 ^b	-18
KTH-2 240 °C	Dibenzothiophene	26	30 ^b	-13
KTH-2 300 °C	-“-	15	17 ^b	-12
KTH-2 360 °C	-“-	2.5 [*]	7 ^b	-64
KTH-3 250 °C	Dibenzothiophene	3.5 [*]	11 ^c	-68
KTH-3 270 °C	-“-	*	15 ^c	-
KTH-3 290 °C	-“-	*	13 ^c	-
KTH-3 320 °C	-“-	*	6 ^c	-
KTH-3 360 °C	-“-	*	0 ^c	-
Naphtha cuts				
C5-149	3-Chlorothiophene	373	480 ^b	-22
95-175	-“-	819	965 ^b	-15
149-232	-“-	2349	3261 ^b	-28

^a Obtained by GC-SCD

^b Obtained by GC-AED

^c Obtained by XRF

^{*} Uncertain results due to too low individual sulphur species concentration

Quantitative results relevant to the examples mentioned in the text are summarised in Table 5.2. In general, the agreement between the results obtained at KTH and the refineries is good although at very low concentrations large discrepancies are observed.

6 Conclusions

In the foreseeable future, the oil refining industry will continue to play an important role in providing gasoline and diesel fuels to the transportation sector worldwide. Present and future developments in oil refining technology are and will be chiefly dedicated to upgrading heavy oil fractions employing environmentally more benign processes and products, the latter urged by progressively tougher legislation.

6.1 Summary of the present thesis

The work presented in this thesis sets out from the activities conducted within the framework of the European Union RESCATS project whose objective was to develop "Poison-resistant catalysts for clean diesel production from LCO". The scientific strategy of the project was based on a two-step catalytic process involving hydrotreating and ring opening. In this thesis, ring opening of naphthenic structures, with special emphasis on the C₅ naphthenic ring in indan, has been investigated employing chiefly bimetallic noble metals-based catalysts. The catalytic performance was evaluated in lab-scale activity tests in an atmospheric pressure fixed bed catalytic reactor operating at a temperature of 325 °C.

The 2 wt.% bimetallic noble metals-based ring-opening catalysts, Pt-Ir in particular, have been prepared employing two different synthesis methods: the microemulsion and the incipient wetness techniques. From an extensive body of physical and chemical characterization results obtained from a multitude of techniques it is evident that there are significant differences with respect to metallic structure properties.

The microemulsion catalysts, in general, display unexpectedly large Pt agglomerates in the approximate range 10-100 nm that are formed during reduction of the metal precursor in the microemulsion phase. Concomitantly, the second metal, Ir or Rh, is shown to remain in a well-dispersed precursor state that is only reduced by thermal treatment with hydrogen following a rather complex pattern as demonstrated by TPR spectra. As seen in corresponding TEM pictures, the resulting catalyst displays severe Pt-Ir phase

segregation. Noteworthy, this observation is not evidenced by dynamic CO pulse chemisorption results with respect to average particle size. This clearly stresses the importance of employing several characterization techniques to obtain complementary information.

In marked contrast, as unanimously evidenced by TEM and dynamic CO pulse chemisorption, catalysts prepared from incipient wetness form small, i.e. approximately 1-3 nm sized, particles upon mild (400 °C) reduction. Corresponding TPR traces, in general, present one to two peaks below 250 °C that are attributable to metals reduction or metals reduction and subsequent hydrogen spillover, the latter holds true where reducible supports are employed, i.e. ceria and zirconia. Quantitative H₂ uptake values obtained during TPR as well as results from XPS indicate that, except for the MgO-based catalyst, complete metals reduction is achieved. Moreover, the TPR traces observed for Pt_{x>0}Ir_{y<100}/CeO₂ catalysts evidence the formation of an alloy phase as the traces are not a sum of the individual monometallic counterparts. Ir is seen to promote the reduction of Pt, which is only possible in case of a close metals intimacy. Conversely, the achievement of an alloy phase is also corroborated by results from XPS studies of spent bimetallic catalysts; when exposed to the atmosphere, Pt in the monometallic Pt catalyst remains unoxidized whereas Pt in the bimetallics, as evidenced by the position of the Pt 4d_{5/2} line, displays an oxidation state indicative of PtO_{1.2}. In addition, quantitative XPS results revealed that the alloy phase is enriched in Ir on the surface.

In fact, for equally metals-loaded catalysts having equal dispersion as determined by dynamic CO chemisorption, the degree of alloying may be deduced implicitly from the results obtained in the atmospheric pressure ring-opening reaction of indan, in particular with respect to the features of the indan conversion versus time on stream curve.

It may be concluded that for Pt-Ir catalysts there is an unambiguous correlation between the catalytic performance in the ring-opening reaction with indan at atmospheric pressure and 325 °C and the surface accessibility of metallic Ir. This is not only because metallic Ir is significantly more active than Pt for cleaving unsubstituted C-C bonds in the five-membered naphthenic-ring structure of indan but also because of its intrinsic hydrogenation/hydrogenolysis properties that mitigate the coking reactions by coke precursor annihilation. Consequently, the 2 wt.% Pt_xIr_y/CeO₂ catalysts that have fairly similar, moderately acid properties, display a linear relationship between the amount of deposited coke and the relative amount of Ir: a higher proportion of Ir, i.e. with an implicitly higher accessibility of surface Ir, results in less coke. Besides, for the 2 wt.%

Pt₅Ir₉₅/support catalysts it was shown that, except for the zirconia-based catalyst, an increasing amount of Brønsted acidity, as determined by the area of the peak-deconvoluted B_{as} band at ca. 1470 cm⁻¹ in the NH₃-DRIFTS spectrum, gives rise to additional coking. In essence, catalyst acidity indeed promotes coking but the atmospheric pressure ring-opening reaction is metals driven and the conversion of indan is mainly governed by the accessibility of surface Ir. Evidently, under atmospheric pressure conditions and with indan as reactant, there is no advantage in employing the Pt-Ir alloy catalysts prepared by the incipient wetness technique.

Extensive sulphur distribution characterization by means of a GC-SCD system has given industrially valuable results regarding sulphur composition in relevant petroleum fractions such as LCO, HDT-LCO and naphtha cuts. Analyses of samples from the catalytic ring-opening reaction at high pressure with the real feed HDT-LCO show that as processing temperature is increased total sulphur decreases but the relative sulphur distribution stays almost unaffected, including the highly refractory 4,6-dimethyldibenzothiophene and C3-DBT's+ species.

Under industrially employed conditions, i.e. 40 bar pressure, the best catalyst candidate emerging from the present thesis and, indeed out of the whole RESCATS project, the 2 wt.% Pt₅Ir₉₅/CeO₂ catalyst prepared from incipient wetness (KTH-3), displays very good diesel quality improvement properties, in particular with respect to cetane boosting. Employing the same conditions, the KTH-3 catalyst brings the cetane index of an industrial feed HDT-LCO stream to higher levels than does a commercially available reference catalyst. Taking into account that industrial partners have promoted its immaterial protection, the output of the present work has to be considered quite successful. When implemented on an industrial scale, the outcome of this work will contribute to better utilization of oil resources and improve refinery economic margins.

6.2 Looking ahead

Today, fossil fuels are a prerequisite of everyday life for people all over the world, in particular in relation to our transportation requirements. Framed against the backdrop of accelerating globalisation, billions of people in developing countries are also aiming at a better standard of living. Fossil fuels are finite resources and to meet the future demands of global welfare under present circumstances, these reservoirs will eventually ebb away. However, before then the excessive emissions of CO₂ and its increasing atmosphere



Figure 6.1 Fossil-fuelled vehicles mounting the Hubbert peak.

concentration will most likely result in serious climate announcements, as CO_2 is known to absorb solar energy.

CO_2 mitigation options such as afforestation, ocean fertilization, liquid CO_2 sequestration (underground or deep ocean storage) are all laudable attempts but, after all, it is sweeping the problem under the carpet. The current energy situation is not sustainable and research must be directed towards finding and producing alternative energy carriers and/or processes for their transformation into appropriate forms of energy. This must be given the highest priority on every political agenda. Many put their hopes to nanotechnology and its promising features to tailor matter on an atomic level. The ultimate goal would be better utilization of the incoming solar flux and the development of technologies based on photolytic splitting of water. In this quest of decisive importance to mankind, the catalysis community certainly has the potential to epoch-making discoveries. The future of the oil industry hinges on long-term planning and the ability to predict and focus on alternative market segments with high profits.

7 Acknowledgments

I would warmly like to thank my supervisors Associate Professor Magali Boutonnet and Professor Sven Järås. Their support and confidence in me have been a great incitement. I very much appreciate the opportunities they have given me to attend conferences and visit their colleagues abroad. It has added to deepening my knowledge and given me valuable contacts.

Among the people within the RESCATS project who assisted me with valuable information and good advice I would particularly like to mention Dr Adriana de Stefanis at CNR, Rome, Dr Juana Frontela Delgado at CEPISA, Madrid and Dr Lorenzo Sassu at Saras, Cagliari.

The six-month-visit to Madrid in 2004 was literally a scientific injection and my deepest gratitude goes to Dr Miguel Pérez Pascual at CEPISA and Professor J.L.G Fierro at ICP for their financial support and, most of all, for their great confidence and generosity, in granting me the use of various kinds of equipment and supplying know-how. Professor Fierro is warmly thanked for personally conducting a large number of XPS and CO FT-IR experiments, and for giving tremendous input. I would also like to express my sincerest gratitude to Dr Bárbara Pawelec and Dr José Maria Mazón Arechederra for their extensive efforts and true concern.

Finally, I'm obliged to Professor François Figueras – I still go back consulting the notes I took at our meetings during my stay at IRC, Lyon in 2002.

I'd like to thank the European Union for providing the financial means through project no. GR01-2000-25596 (RESCATS) to make the first three years of my PhD studies possible.

All present and former colleagues at Chemical Technology and Chemical Reaction Engineering at KTH, Stockholm, are dearly acknowledged.

Special thanks to:

- ★ Tomas Östberg and Bo Karlsson in the workshop for their help with construction of experimental equipment
- ★ Associate Professor Lars Pettersson for valuable advice
- ★ Lars-Peter Wiktorsson for advice on practical matters in technical laboratory work
- ★ Dr Christina Hörnell for helping me not only with the linguistic quality of paper manuscripts and theses but also for giving constructive scientific comments
- ★ Inga Groth for assistance with the characterization instruments at the department
- ★ Otto von Krusenstierna for sharing with me his knowledge, experience and scientific enthusiasm
- ★ My room-mate and sparring partner Henrik Birgersson, whose good companionship I've enjoyed in everyday work as well as during the many travels abroad
- ★ A very special thank to Thomas Nordgreen for friendship and unfailing support

Last, but not least, I would like to thank my fiancée Emma and my parents for their help and encouragement during the past five years.

Nomenclature

ASTM	American Society for Testing and Materials
BE	Binding Energy
BT	BenzoThiophene
CI	Cetane Index
CN	Cetane Number
DBT	DiBenzoThiophene
DRIFTS	Diffuse Reflectance Infrared Fourier Transform Spectroscopy
EDX	Energy Dispersive X-ray (spectroscopy)
FCC	Fluid Catalytic Cracking
FID	Flame Ionization Detector
FT-IR	Fourier Transform InfraRed (spectroscopy)
GC	Gas Chromatography
HDT-LCO	HyDroTreated Light Cycle Oil
IW	Incipient Wetness
LCO	Light Cycle Oil
LHSV	Liquid Hourly Space Velocity
ME	Microemulsion
MS	Mass Spectroscopy
PEGDE	PentaEthylene Glycol mono <i>n</i> -Dodecyl Ether
PM	Particulate Matter
RESCATS	acronym for the European Union project “Poison-resistant catalysts for clean diesel production from LCO”
SCD	Sulphur Chemiluminescence Detector
SEM	Scanning Electron Microscopy
SIM-DIS	Simulated Distillation
SRO	Selective Ring Opening
TEM	Transmission Electron Microscopy
TG	Thermal gravimetry
TPO	Temperature Programmed Oxidation

TPR	Temperature Programmed Reduction
XPS	X-ray Photoelectron Spectroscopy
XRD	X-ray Diffraction
XRF	X-ray Fluorescence (spectroscopy)
WABT	Weighted Average Bed Temperature

References

- [1] S.A. Sherif, F. Barbir, T.N. Veziroglu, *Sol. Energy* 78 (2005) 647.
- [2] K. Kaygusuz, *Energ. Source.* 26 (2004) 95.
- [3] Z. Şen, *Prog. Energ. Combust.* 30 (2004) 367.
- [4] Z. Kowalik, *Oceanologia* 46 (2004) 291.
- [5] G.P. Harrison, A.R. Wallace, *Renew. Energ.* 30 (2005) 1801.
- [6] A.S. Bahaj, L. Myers, *Renew. Energ.* 29 (2004) 1931.
- [7] E. Barbier, *Renew. Sust. Energ. Rev.* 6 (2002) 3.
- [8] M. Balat, G. Ayar, *Energ. Source.* 27 (2005) 931.
- [9] P. Tseng, J. Lee, P. Friley, *Energy* 30 (2005) 2703.
- [10] K.S. Deffeyes, *Hubbert's peak - the impending world oil shortage*, Princeton University Press, New Jersey, 2003.
- [11] R.A. Kerr, *Science* 281 (1998) 1128.
- [12] BP Statistical review of world energy 2005, http://www.bp.com/liveassets/bp_internet/globalbp/globalbp_uk_english/publications/energy_reviews_2005/STAGING/local_assets/downloads/pdf/statistical_review_of_world_energy_full_report_2005.pdf, accessed 2005-11-02.
- [13] CONCAWE review 11(2) (2002) 8.
- [14] M. Booth, J.G. Buglass, J.F. Unsworth, *Top. Catal.* 16/17 (2001) 39.
- [15] H. Hoshi, H. Hayashi, *Toyota Technical Review* 53 (2004) 10.
- [16] B. Williams, *Oil Gas J.* 101(31) (2003) 20.
- [17] B.A. Stankiewicz, *Nature* 426 (2003) 360.
- [18] C. Hall, P. Tharakan, J. Hallock, C. Cleveland, M. Jefferson, *Nature* 426 (2003) 318.
- [19] M.E. Dry, *Catal. Today* 71 (2002) 227.
- [20] E.D. Sloan Jr., *Nature* 426 (2003) 353.
- [21] D. Nakamura, *Oil Gas J.* 101(49) (2003) 64.
- [22] I.V. Babich, J.A. Moulijn, *Fuel* 82 (2003) 607.
- [23] J.H. Gary, G.E. Handwerk, *Petroleum refining, technology and economics* 3rd ed., Marcel Dekker, New York, 1994.
- [24] M. Marafi, A. Stanislaus, J. Hazard. Mater. B101 (2003) 123.
- [25] <http://www.acea.be/ASB20/axidownloads20s.nsf/Category2ACEA/>

D3D0E3E056E803B2C125702F004A7D11/\$File/DIESEL-PC-90-04.pdf,
accessed 2005-11-02.

- [26] G.C. Laredo, S. Leyva, R. Alvarez, M.T. Mares, J. Castillo, J.L. Cano, *Fuel* 81 (2002) 1341.
- [27] P. Courty, J.F. Gruson, *Oil Gas Sci. Technol.* 56 (2001) 515.
- [28] J.A. Moulijn, M. Makkee, A. van Diepen, *Chemical process technology*, John Wiley & Sons Ltd, Chichester, 2001.
- [29] P. Greening, *Top. Catal.* 16/17 (2001) 5.
- [30] J. Beens, U.A.Th. Brinkman, *TrAC-Trend. Anal. Chem.* 19 (2000) 260.
- [31] J. Phipps, The Institute of Petroleum (IP)'s Petroleum Review, May (2001) 40.
- [32] K. Owen, T. Coley, *Automotive fuels reference book 2nd ed.*, Society of automotive engineers, Inc., Warrendale, 1995.
- [33] D. Karonis, E. Lois, S. Stournas, F. Zannikos, *Energ. Fuel.* 12 (1998) 230.
- [34] J.B. Heywood, *Internal combustion engine fundamentals*, McGraw-Hill book company, Singapore, 1988.
- [35] European Union Directive 2003/17/EC.
- [36] F.L. Plantenga, R.G. Leliveld, *Appl. Catal. A-Gen.* 248 (2003) 1.
- [37] D.N. Nakamura, *Oil Gas J.* 102(39) (2004) 48.
- [38] E. Fridell, H. Persson, L. Olsson, B. Westerberg, A. Amberntsson, M. Skoglundh, *Top. Catal.* 16/17 (2001) 133.
- [39] *Kemivärlden* 8 (2003) 5.
- [40] *Kemivärlden* 9 (2003) 5.
- [41] J.H. Sinfelt, *Catal. Lett.* 9 (1991) 159.
- [42] B.H. Cooper, B.B.L. Donnis, *Appl. Catal. A-Gen.* 137 (1996) 203.
- [43] W.R. Patterson, J.J. Rooney, *Catal. Today* 12 (1992) 113.
- [44] J.M. Dartigues, A. Chambellan, S. Corolleur, F.G. Gault, A. Renouprez, B. Moraweck, P. Bosch-Giral, G. Dalmai-Imelick, *Nouv. J. Chim.* 3 (1979) 591.
- [45] F. Weisang, F.G. Gault, *J. Chem. Soc. Chem. Comm.* 11 (1979) 519.
- [46] D. Teschner, Z. Paál, *React. Kinet. Catal. L.* 68 (1999) 25.
- [47] D. Teschner, D. Duprez, Z. Paál, *J. Mol. Catal. A-Chem.* 179 (2002) 201.
- [48] V. Amir-Ebrahimi, F. Garin, F. Weisang, F.G. Gault, *Nouv. J. Chim.* 3 (1979) 529.
- [49] K. Foger, J.R. Anderson, *J. Catal.* 59 (1979) 325.
- [50] L.M. Kustov, A.Y. Stakheev, T.V. Vasina, O.V. Masloboishchikova, E.G. Khelkovskaya-Sergeeva, P. Zeuthen, *Stud. Surf. Sci. Catal.* 138 (2001) 307.
- [51] D. Kubička, N. Kumar, P. Mäki-Arvela, M. Tiitta, V. Niemi, T. Salmi, D.Y. Murzin, *J. Catal.* 222 (2004) 65.

- [52] D. Kubička, N. Kumar, P. Mäki-Arvela, M. Tiitta, V. Niemi, H. Karhu, T. Salmi, D.Y. Murzin, *J. Catal.* 227 (2004) 313.
- [53] G.B. McVicker, M. Daage, M.S. Touvelle, C.W. Hudson, D.P. Klein, W.C. Baird Jr., B.R. Cook, J.G. Chen, S. Hantzer, D.E.W. Vaughan, E.S. Ellis, O.C. Feeley, *J. Catal.* 210 (2002) 137.
- [54] M. Santikunaporn, J.E. Herrera, S. Jongpatiwut, D.E. Resasco, W.E. Alvarez, E.L. Sughrue, *J. Catal.* 228 (2004) 100.
- [55] A. Corma, V. González-Alfaro, A.V. Orchillés, *J. Catal.* 200 (2001) 34.
- [56] H.B. Mostad, T.U. Riis, O.H. Ellestad, *Appl. Catal.* 63 (1990) 345.
- [57] M.A. Arribas, P. Concepción, A. Martínez, *Appl. Catal. A-Gen.* 267 (2004) 111.
- [58] M.A. Arribas, A. Corma, M.J. Díaz-Cabañas, A. Martínez, *Appl. Catal. A-Gen.* 273 (2004) 277.
- [59] E. Rodríguez-Castellón, J. Mérida-Robles, L. Díaz, P. Maireles-Torres, D.J. Jones, J. Rozière, A. Jiménez-López, *Appl. Catal. A-Gen.* 260 (2004) 9.
- [60] H. Yasuda, T. Sato, Y. Yoshimura, *Catal. Today* 50 (1999) 63.
- [61] D. Eliche-Quesada, J. Mérida-Robles, P. Maireles-Torres, E. Rodríguez-Castellón, A. Jiménez-López, *Langmuir* 19 (2003) 4985.
- [62] K. Sato, Y. Iwata, Y. Miki, H. Shimada, *J. Catal.* 186 (1999) 45.
- [63] P.A. Rautanen, J.R. Aittamaa, A.O.I. Krause, *Chem. Eng. Sci.* 56 (2001) 1247.
- [64] P. Da Costa, J-L. Lemberon, C. Potvin, J-M. Manoli, G. Perot, M. Breysse, G. Djega-Mariadassou, *Catal. Today* 65 (2001) 195.
- [65] A.T. Townsend, J. Abbot, *Appl. Catal. A-Gen.* 90 (1992) 97.
- [66] K. Sato, Y. Iwata, T. Yoneda, A. Nishijima, Y. Miki, H. Shimada, *Catal. Today* 45 (1998) 367.
- [67] J.L. Lemberon, A. Baudon, M. Guisnet, N. Marchal, S. Mignard, *Stud. Surf. Sci. Catal.* 106 (1997) 129.
- [68] S. Jongpatiwut, Z. Li, D.E. Resasco, W.E. Alvarez, E.L. Sughrue, G.W. Dodwell, *Appl. Catal. A-Gen.* 262 (2004) 241.
- [69] A. Corma, A. Martínez, V. Martínez-Soria, *J. Catal.* 169 (1997) 480.
- [70] M. Jacquin, D.J. Jones, J. Rozière, S. Albertazzi, A. Vaccari, M. Lenarda, L. Storaro, R. Ganzerla, *Appl. Catal. A-Gen.* 251 (2003) 131.
- [71] M. Jacquin, D.J. Jones, J. Rozière, A. Jiménez López, E. Rodríguez-Castellón, J.M. Trejo Menayo, M. Lenarda, L. Storaro, A. Vaccari, S. Albertazzi, *J. Catal.* 228 (2004) 447.
- [72] K. Ito, Y. Kogasaka, H. Kurokawa, M. Ohshima, K. Sugiyama, H. Miura, *Fuel Process. Technol.* 79 (2002) 77.
- [73] K.M. Reddy, C. Song, *Catal. Today* 31 (1996) 137.

- [74] S. Albertazzi, G. Busca, E. Finocchio, R. Glöckler, A. Vaccari, *J. Catal.* 223 (2004) 372.
- [75] Y. Miki, Y. Sugimoto, *Fuel Process. Technol.* 43 (1995) 137.
- [76] M.A. Arribas, A. Martínez, *Stud. Surf. Sci. Catal.* 130 (2000) 2585.
- [77] M.A. Arribas, A. Martínez, *Appl. Catal. A-Gen.* 230 (2002) 203.
- [78] F.E. Shephard, J.J. Rooney, *J. Catal.* 3 (1964) 129.
- [79] N. Davidova, V. Penčev, L. Beránek, *Collect. Czech. Chem. C.* 33 (1968) 1229.
- [80] V. Pentshev, N. Davidova, *Brennst. Chem.* 49 (1968) 33.
- [81] G. Guidot, J.E. Germain, *Ann. Chim. France* 9 (1974) 191.
- [82] V.I. Savchenko, I.A. Makaryan, V.G. Dorokhov, *Platinum Metals Rev.* 41 (1997) 176.
- [83] M.S. Touvelle, G.B. McVicker, M. Daage, S.S. Hantzer, C.W. Hudson, D.P. Klein, D.E.W. Vaughan, E.S. Ellis, J.G. Chen, WO Patent 97/09290 (1997), to Exxon Research and Engineering Company.
- [84] S. Hantzer, M.S. Touvelle, J.G. Chen, US Patent 5 811 624 (1998), to Exxon Research and Engineering Company.
- [85] G.B. McVicker, J.J. Schorfheide, W.C Baird Jr., M.S. Touvelle, M. Daage, D.P. Klein, E.S. Ellis, D.E.W. Vaughan, J. Chen, S.S. Hantzer, US Patent 6 103 106 (2000), to Exxon Research and Engineering Company.
- [86] W.C. Baird Jr., D.P. Klein, J.G. Chen, G.B. McVicker, WO Patent 02/07881 A1 (2002), to ExxonMobil Research and Engineering Company.
- [87] W.C. Baird Jr., D.P. Klein, J.G. Chen, G.B. McVicker, US Patent 6 683 020 B2 (2004), to ExxonMobil Research and Engineering Company.
- [88] J.C. Rasser, W.H. Beindorff, J.J.F. Scholten, *J. Catal.* 59 (1979) 211.
- [89] J. Barbier, E. Churin, P. Marecot, *J. Catal.* 126 (1990) 228.
- [90] O.B. Yang, S.I. Woo, I.C. Hwang, *Catal. Lett.* 19 (1993) 239.
- [91] Platinum Today (website of Johnson Matthey Precious Metals Marketing), http://www.platinum.matthey.com/prices/price_charts.html, accessed 2005-11-02.
- [92] T. Fujikawa, K. Idei, T. Ebihara, H. Mizuguchi, K. Usui, *Appl. Catal. A-Gen.* 192 (2000) 253.
- [93] F. Figueras, J. Palomeque, S. Loridant, C. Fèche, N. Essayem, G. Gelbard, *J. Catal.* 226 (2004) 25.
- [94] A.A.G. Tomlinson, *J. Porous Mat.* 5 (1998) 259.
- [95] M. Boutonnet, J. Kizling, P. Stenius, G. Maire, *Colloid. Surface.* 5 (1982) 209.
- [96] R. Touroude, P. Girard, G. Maire, J. Kizling, M. Boutonnet-Kizling, P. Stenius, *Colloid. Surface.* 67 (1992) 9.
- [97] J. Xue, Y.-J. Huang, J.A. Schwarz, *Appl. Catal.* 42 (1988) 61.

- [98] J.H. Sinfelt, *Catal. Today* 53 (1999) 305.
- [99] J.H. Sinfelt, G.H. Via, *J. Catal.* 56 (1979) 1.
- [100] A. Zecua-Fernández, A. Gómez-Cortés, A.E. Cordero-Borboa, A. Vázquez-Zavala, *Appl. Surf. Sci.* 182 (2001) 1.
- [101] R.L. Garten, J.H. Sinfelt, *J. Catal.* 62 (1980) 127.
- [102] J.L. Carter, G.B. McVicker, W. Weissman, W.S. Kmak, J.H. Sinfelt, *Appl. Catal.* 3 (1982) 327.
- [103] G.B. McVicker, J.J. Ziemiak, *Appl. Catal.* 14 (1985) 229.
- [104] S.C. Chan, S.C. Fung, J.H. Sinfelt, *J. Catal.* 113 (1988) 164.
- [105] J.H. Sinfelt, G.H. Via, F.W. Lytle, *J. Chem. Phys.* 76 (1982) 2779.
- [106] A. El Biyyadh, M. Guérin, C. Kappenstein, D. Bazin, H. Dexpert, *J. Chim. Phys.* 86 (1989) 1751.
- [107] N. Wagstaff, R. Prins, *J. Catal.* 59 (1979) 446.
- [108] K. Foger, H. Jaeger, *J. Catal.* 67 (1981) 252.
- [109] A.C. Faro Jr., M.E. Cooper, D. Garden, C. Kemball, *J. Chem. Res-S.* 5 (1983) 110.
- [110] X.-K. Wang, J.A. Schwarz, *Appl. Catal.* 18 (1985) 147.
- [111] Y.-J. Huang, J. Xue, J.A. Schwarz, *J. Catal.* 111 (1988) 59.
- [112] Y.-J. Huang, S.C. Fung, W.E. Gates, G.B. McVicker, *J. Catal.* 118 (1989) 192.
- [113] S. Subramanian, J.A. Schwarz, *Appl. Catal.* 68 (1991) 131.
- [114] S. Subramanian, J.A. Schwarz, *Appl. Catal.* 74 (1991) 65.
- [115] J.T. Richardson, *Principles of catalyst development*, Plenum Press, New York, 1989.
- [116] *Chem. Eng. News* 83(19) (2005) 39.
- [117] B. Folkesson, *Acta Chem. Scand.* 27 (1973) 287.
- [118] J.F. Moulder, W.F. Stickle, P.E. Sobol, K.D. Bomben, *Handbook of X-ray photoelectron spectroscopy*, Perkin-Elmer Corporation, Minnesota, 1992.
- [119] F. Locatelli, B. Didillon, D. Uzio, G. Niccolai, J.P. Candy, J.M. Basset, *J. Catal.* 193 (2000) 154.
- [120] M. Peuckert, *Electrochim. Acta* 29 (1984) 1315.
- [121] A. Talo, J. Lahtinen, P. Hautojärvi, *Appl. Catal. B-Environ.* 5 (1995) 221.
- [122] J.Z. Shyu, K. Otto, *Appl. Surf. Sci.* 32 (1988) 246.
- [123] S. Penner, G. Rupprechter, H. Sauer, D.S. Su, R. Tessedri, R. Podloucky, R. Schlögl, K. Hayek, *Vacuum* 71 (2003) 71.
- [124] G. Schoen, *J. Electron Spectrosc.* 1 (1972) 377.
- [125] T. Huizinga, H.F.J. Van't Blik, J.C. Vis, R. Prins, *Surf. Sci.* 135 (1983) 580.
- [126] C. de Leitenburg, A. Trovarelli, J. Kašpar, *J. Catal.* 166 (1997) 98.
- [127] W. Curtis Conner Jr., J.L. Falconer, *Chem. Rev.* 95 (1995) 759.

- [128] S. Bernal, J.J. Calvino, J.M. Gatica, C. Larese, C. López-Cartes, J.A. Pérez-Omil, *J. Catal.* 169 (1997) 510.
- [129] H. Yoshitake, Y. Iwasawa, *J. Phys. Chem.* 96 (1992) 1329.
- [130] F. Fajardie, J.-F. Tempere, J.-M. Manoli, G. Djega-Mariadassou, G. Blanchard, *J. Chem. Soc. Faraday T.* 94 (1998) 3727.
- [131] J. Le Bars, J.C. Vedrine, A. Auroux, S. Trautmann, M. Baerns, *Appl. Catal. A-Gen.* 88 (1992) 179.
- [132] K.D. Jandt, *Surf. Sci.* 491 (2001) 303.
- [133] J.M.L. Penninger, H.W. Slotboom, *Recl. Trav. Chim. Pay. B.* 92 (1973) 513.
- [134] D.A. Skoog, F.J. Holler, T.A. Nieman, *Principles of instrumental analysis* 5ed., Harcourt Brace & Company, Orlando, 1998.
- [135] R.W. Rice, D.C. Keptner, *Appl. Catal. A-Gen.* 262 (2004) 233.
- [136] A. Charron, C. Kappenstein, M. Guérin, Z. Paál, *Phys. Chem. Chem. Phys.* 1 (1999) 3817.
- [137] J. Barbier, E. Churin, J.M. Parera, J. Riviere, *React. Kinet. Catal. L.* 29 (1985) 323.
- [138] *Annual book of ASTM standards*, section 5, volume 05.02, Baltimore, 2004.
- [139] L. Sassu, C. Delitala, L. Leoni, R. Baratti, S. Melis, *Chem. Eng. Trans.* 3 (2003) 491.
- [140] J.P. van den Berg, J.P. Lucien, G. Germaine, G.L.B. Thielemans, *Fuel Process. Technol.* 35 (1993) 119.
- [141] P.T. Vasudevan, J.L.G. Fierro, *Catal. Rev.* 38 (1996) 161.
- [142] H.R. Reinhoudt, R. Troost, A.D. van Langeveld, S.T. Sie, J.A.R. van Veen, J.A. Moulijn, *Fuel Process. Technol.* 61 (1999) 133.
- [143] K.G. Knudsen, B.H. Cooper, H. Topsøe, *Appl. Catal. A-Gen.* 189 (1999) 205.
- [144] R. Galiasso Tailleur, J. Ravigli, S. Quenza, N. Valencia, *Appl. Catal. A-Gen.* 282 (2005) 227.
- [145] M.V. Landau, *Catal. Today* 36 (1997) 393.
- [146] M. Macaud, A. Milenkovic, E. Schulz, M. Lemaire, M. Vrinat, *J. Catal.* 193 (2000) 255.
- [147] R. L. Benner, D.H. Stedman, *Anal. Chem.* 61 (1989) 1268.
- [148] R.L. Shearer, *Chem. Anal.* 131 (1995) 35.
- [149] R.S. Hutte, in: E.R. Adlard (Ed.), *Chromatography in the petroleum industry*, Elsevier, Amsterdam, 1995, pp. 201-229.